

AD-A274 889



2

PL-TR-92-2330

Environmental Research Papers, No. 1113

A MODELING STUDY OF THE MESOCYCLONE

Paul R. Desrochers

4 December 1992

DTIC
S ELECTE D
E JAN 11 1994

APPROVED FOR PUBLIC RELEASE; DISTRIBUTION UNLIMITED



PHILLIPS LABORATORY

Directorate of Geophysics

AIR FORCE MATERIEL COMMAND

HANSCOM AIR FORCE BASE, MA 01731-5000

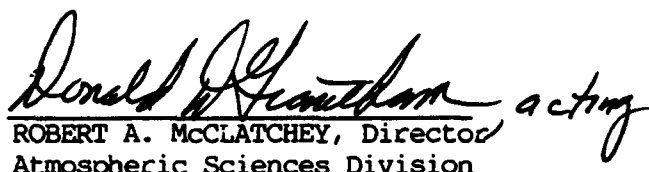
50p6 **94-01115**

94 1 10 107

"This technical report has been reviewed and is approved for publication"



DONALD A. CHISHOLM, Chief
Atmospheric Prediction Branch

 acting

ROBERT A. McCLATCHEY, Director
Atmospheric Sciences Division

This report has been reviewed by the ESC Public Affairs Office (PA) and is releasable to the National Technical Information Service (NTIS).

Qualified requestors may obtain additional copies from the Defense Technical Information Center (DTIC). All others should apply to the National Technical Information Service (NTIS).

If your address has changed, if you wish to be removed from the mailing list, or if the addressee is no longer employed by your organization, please notify PL/TSI, 29 Randolph Road, Hanscom AFB, MA 01731-3010. This will assist us in maintaining a current mailing list.

Do not return copies of this report unless contractual obligations or notices on a specific document requires that it be returned.

REPORT DOCUMENTATION PAGEForm Approved
OMB No. 0704-0188

Public reporting burden for this collection of information is estimated to average 1 hour per response, including the time for reviewing instructions, searching existing data sources, gathering and maintaining the data needed, and completing and reviewing the collection of information. Send comments regarding this burden estimate or any other aspect of this collection of information, including suggestions for reducing this burden, to Washington Headquarters Services, Directorate for Information Operations and Reports, 1215 Jefferson Davis Highway, Suite 1204, Arlington, VA 22202-4302, and to the Office of Management and Budget, Paperwork Reduction Project (0704-0188), Washington, DC 20503.

1. AGENCY USE ONLY (Leave blank)**2. REPORT DATE**

4 December 1992

3. REPORT TYPE AND DATES COVERED

Scientific Interim

4. TITLE AND SUBTITLE

A Modeling Study of the Mesocyclone

5. FUNDING NUMBERS

PE: 63707F

PR: 2781

TA: 01

WU: 06

6. AUTHOR(S)

Paul R. Desrochers

7. PERFORMING ORGANIZATION NAME(S) AND ADDRESS(ES)Phillips Lab (GPAP)
Hanscom Air Force Base
Massachusetts 01731-5000**8. PERFORMING ORGANIZATION
REPORT NUMBER**

PL-TR-92-2330

ERP, No. 1113

9. SPONSORING/MONITORING AGENCY NAME(S) AND ADDRESS(ES)**10. SPONSORING/MONITORING
AGENCY REPORT NUMBER****11. SUPPLEMENTARY NOTES****12a. DISTRIBUTION/AVAILABILITY STATEMENT**

Approved for public release; distribution unlimited

12b. DISTRIBUTION CODE**13. ABSTRACT (Maximum 200 words)**

The mesocyclone is a strongly-rotating column of air associated with the updraft of a severe thunderstorm. The size and shape of the phenomenon allows ready detection with a single Doppler radar. Quantitative evaluation of the mesocyclone has been shown to be useful for the prediction of large hail and tornadoes. Accuracy in mesocyclone interpretation is of course critical to these endeavors.

A limitation with single-Doppler observation of the mesocyclone is that the flow field is measured directly in only one dimension. Therefore, the shape and spatial variation of intensity can be difficult to determine. For this reason, it is common practice to assume the mesocyclone flow is circularly symmetric when interpreting the single-Doppler image. The problem is that mesocyclone flows are generally not circular, and the deviation from circular can be considerable.

This report presents an improved model for the interpretation of single-Doppler mesocyclone observations. The model describes an elliptical flow pattern of any eccentricity. Some examples of highly distorted, single-Doppler, mesocyclone flows are presented which are well simulated by the model.

14. SUBJECT TERMS

Mesocyclone modeling; Elliptical mesocyclones; Doppler radar interpretation

15. NUMBER OF PAGES

52

16. PRICE CODE**17. SECURITY CLASSIFI-
CATION OF REPORT**

UNCLASSIFIED

**18. SECURITY CLASSIFI-
CATION OF THIS PAGE**

UNCLASSIFIED

**19. SECURITY CLASSIFI-
CATION OF ABSTRACT**

UNCLASSIFIED

**20. LIMITATION OF
ABSTRACT**

SAR

Contents

1. INTRODUCTION	1
2. THE CLASSICAL MESOCYCLONE MODEL	2
3. NON-CIRCULAR ROTATION AND NON-SYMMETRICAL FLOWS	5
3.1 Rotation in an Elliptical Flow	9
3.2 Kinematics of the Model Rotational Flow	14
3.3 Rotational Kinetic Energy	19
3.4 Excess Rotational Kinetic Energy	21
4. DIVERGENCE SCENARIOS FOR ELLIPTICAL FLOW	23
4.1 Uniform Divergence	26
4.2 Uniform Convergence and Rotation	26
4.3 Non-Uniform Convergence	33
5. DISCUSSION AND CONCLUSIONS	35
References	43

DTIC QUALITY INSPECTED 5

Accession For	
NTIS CRA&I	<input checked="" type="checkbox"/>
DTIC TAB	<input type="checkbox"/>
Unannounced	<input type="checkbox"/>
Justification	
By	
Distribution /	
Availability Codes	
Dist	Avail and/or Special
A-1	

Illustrations

1. Theoretical Mesocyclone Profile Described by a Rankine Combined Vortex	3
2. Mesocyclone Appearance as seen by Single Doppler Radar for a Circular RCV Flow Containing Equal Magnitudes of Vorticity and Convergence	4
3. The Associated Vorticity and Divergence (convergence) Fields for a Circular, RCV Flow Associated with the Example in Figure 2	6
4. B-scan Format of the Del City OK, Storm of 20 May 1977 at 1827 CST	7
5. Same as Figure 4, but for the Radar Volume Scan Beginning at 1832 CST	8
6. Elliptical Mesocyclone Model Setup	10
7. Examples of the Elliptical Mesocyclone Model for the Condition Of Pure Rotation	12
8. Detectable Shear, by Single Doppler Radar, as a Function of the Mesocyclone (ellipse) Orientation with Respect to the Radar	15
9. Comparison of the Model Output for Pure Rotation to a Real Life Example from the Del City Storm	16
10. Presentations of the Vorticity Field for an Elliptical Mesocyclone Flow as a Function of the Stretch Factor	17
11. An Example of How the Velocity Field in the Potential Flow Area of an Elliptically-shaped Mesocyclone Would Have to Vary to Have Zero Anticyclonic Vorticity	20
12. Variation of ERKE as a Function of Ellipse Stretch Factor and ERKE Shear Threshold	22
13. Variation of ERKE with Feature Eccentricity and Vorticity	24

14. Ratio of Circle ERKE to the True ERKE of an Ellipse as a Function of Stretch Factor and Feature Orientation	25
15. Example of the Divergence Field Produced by the Elliptical Mesocyclone Model	27
16. Examples of the Elliptical Mesocyclone Model for the Condition of Pure Divergence	28
17. Examples of the Elliptical Mesocyclone Model Velocity Field for Equal Magnitudes of Convergence and Vorticity Inside the Core	30
18. Comparison of the Elliptical Mesocyclone Model (a) to an Example From the Del City Storm (b)	32
19. Fields of the Convergence Term for Vorticity Tendency (a), Vertical Vorticity (b), and Low Level Winds (c) Determined From Multiple-Doppler Analysis of the Del City Storm at 1826 CST and 1.3 km AGL	34
20. An Estimation of the Divergence Field for the 1826 Del City Example	36
21. The Divergence Field Contributing to the Convergence Term of Vorticity Tendency Shown in Figure 20	37
22. The Induced Vorticity Field Associated with the Non-uniform Inflow of Figure 20	38
23. The Total Model Vorticity Field from the Combination of a Uniform Vorticity Field For Rotation with the Vorticity Induced by the Non-uniform Inflow	39
24. An Example of how the Model can be used to Explain Complicated Patterns of Vorticity and Divergence in the Mesocyclone Core	40

Preface

I am grateful to Dr. F. Ian Harris of Hughes/STX who provided helpful suggestions and comments during the development of this work.

A Modeling Study of the Mesocyclone

1. INTRODUCTION

A well-known characteristic of supercell-type storms is a deep, wide region (≥ 3 km) of persistent (≥ 5 minutes) rotation (shear $\geq 0.005/\text{s}$) known as the mesocyclone. Storms exhibiting this degree of organized rotation are extremely dangerous. Almost all produce severe weather of one kind or another. It is fortuitous that the mesocyclone produces a distinct signature in the single-Doppler velocity field that is not only easy to recognize by eye, but is generally straightforward to detect through automated means. The single-Doppler mesocyclone signature is now considered to be a most valuable warning criterion for severe weather.

Doppler radar only senses the component of motion that is directed along the radar beam. This limited perspective means that a rotating mass, larger in width than the radar beam, will be sensed directly only along a cross section. With only one dimension of the rotating feature well resolved, the total shape and velocity distribution of the rotating area is not easily obtained. For convenience, and for lack of a better model, the mesocyclone is generally assumed to be circular, with the flow varying according to a Rankine-combined vortex (RCV) as first proposed by Lhermitte (1964), herein referred to as the *circular mesocyclone model*.

The assumption of circular flow is a reasonable first-order approximation, and is supported by numerous observations. Circularity is, in fact, a cornerstone of existing detection and evaluation techniques. Donaldson (1970) proposed criteria² for positive single-Doppler identification of a mesocyclone based on a circularity assumption. These criteria, having proven effective during operations, were built in one form or another into automated mesocyclone detection algorithms (for example, Wieler,³ and Zrnic' et al.,⁴). Circularity is assumed in automated techniques for hail prediction (for example, Witt and Nelson,⁵) and tornado prediction (Desrochers and Donaldson,⁶). The success of severe weather evaluators that use mesocyclone related parameters depends largely on the validity of the model used to extract the mesocyclone information.

Mesocyclones are not necessarily circular. There is evidence to support this in multiple-Doppler studies (for example, Brandes,⁷), where the mesocyclone sometimes appears elongated. Mesocyclone signatures from single-Doppler observations often differ in detail from the ideal proposed by the circular model. Some of these irregularities can be explained by embedded vortices within a general mesocyclone flow, as modeled nicely by Brown and Wood⁸. Other irregularities are more difficult to explain, except to say they must be associated with a distorted or non-uniform flow field. The results of such distortions is the topic of this investigation.

As a starting point, it is useful to examine the circular-model kinematics to see how well they agree with the three-dimensional (3-D) flow field of a supercell-type updraft. From there, alternative models of the mesocyclone will be examined. Specifically, we will examine an elliptical flow field to show how it can better explain some of the irregularities observed in the single-Doppler flow.

2. THE CLASSICAL MESOCYCLONE MODEL

The velocity distribution of the circular mesocyclone model is shown in Figure 1a. This model consists of two flow regimes: an inner or "core" region, and an outer or "potential flow". Flow within the core varies linearly with distance from the mesocyclone center and is described by

$$v/r = C_1, \quad (1)$$

where (v) is the velocity at any radius (r) inside the core, and $C_1 = V / R$, a constant related by the peak velocity (V) found at the mesocyclone core radius (R) that separates the solid body and potential flows. Conversely, flow within the potential flow region is given by

$$v r = C_2 = V R. \quad (2)$$

When radar resolution permits, (as it generally does for flows the size of mesocyclones) the mesocyclone is seen as a velocity couplet, with the flow defined well at only the two points where the radar-relative incoming and outgoing velocities are greatest. An example of a couplet for pure rotation is shown in Figure 1b, where the radar viewpoint is from the bottom of the page. For rotation, the model describes a flow that rotates as a solid body inside the core region. Pure rotation may exist at one or more levels between 2 and 7 km AGL.

At most elevations there is a component of divergence associated with the mesocyclonic flow. This results in a clockwise rotation of the couplet in Figure 1b for convergence and counterclockwise for divergence. The orientation angle of the velocity peaks ϕ , relative to the radar beam, is 0° for pure rotation, -90° for pure convergence, and 90° for pure divergence. At the mesocyclone core radius, components of velocity associated with rotation (V_r) and divergence (V_d) are given by $V_o \cos(\phi)$ and $V_o \sin(\phi)$, respectively, where V_o is the average of the radar observed velocity couplet velocity maxima. Figure 2 shows a mesocyclone with $\phi = -45^\circ$, where the component of velocity due to inflow is equal to the component associated with rotation.

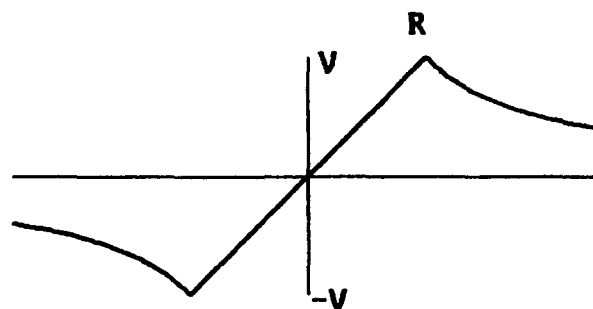
Pure convergence may exist at low levels of a storm, but generally not as part of a circular, mesocyclonic flow. At the storm top, however, signatures of pure divergence in an apparently circular flow are common.

Vorticity and divergence fields are simple and straightforward to evaluate for a circular mesocyclone flow. The circular model equations describe a flow field in which magnitudes of velocity are a function only of range from the vortex center and not a function of direction. Consider first a purely rotational flow where the velocity varies according to Eqs.(1) and (2) and the total component of velocity is normal to the mesocyclone radius arm. With the mesocyclone examined in a Cartesian coordinate system defined by directions x and y , and velocity components u_x and u_y , then, in the mesocyclone core, $\partial u_y / \partial x$ is positive at any given point for cyclonic rotation, and equal in magnitude but opposite in sign to $\partial u_x / \partial y$. Therefore, within the core region,

$$\text{Vorticity } (\nabla \times \vec{V}) = 2 \partial u_y / \partial x = 2 V_o \cos(\phi) / R = 2 V_r / R. \quad (3)$$

Vorticity is constant within the core region and equal to twice the peak mesocyclone rotational velocity divided by the core radius.

a)



b)

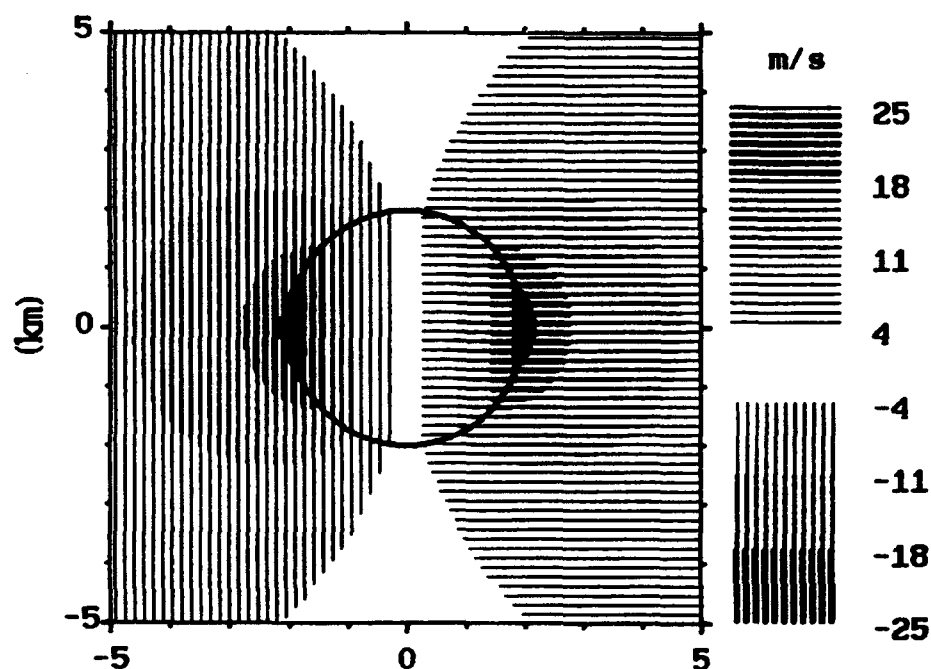


Figure 1. Velocity Distribution for a Circular, Axisymmetric, Rankine-Combined Vortex (RCV) Mesocyclone Flow. a) Velocity magnitude as a function of distance from the mesocyclone center. The mesocyclone radius, called the core radius (R), corresponds to the locations of peak velocity directed towards ($-$) and away from ($+$) the radar ($\pm V$). b) Theoretical mesocyclone appearance for a purely rotational flow as seen by single Doppler radar, for a radar located in the direction towards the bottom of the page. Contour levels are as indicated except that radial velocities within 7.5 percent of maximum or minimum are indicated by the solid black contour. The circle drawn indicates the mesocyclone ring of maximum velocity that defines the core. Pure rotation is indicated by inbound and outbound velocity peaks that are at the same range from the radar. This is defined by a velocity peaks' orientation angle (ϕ) of 0° .

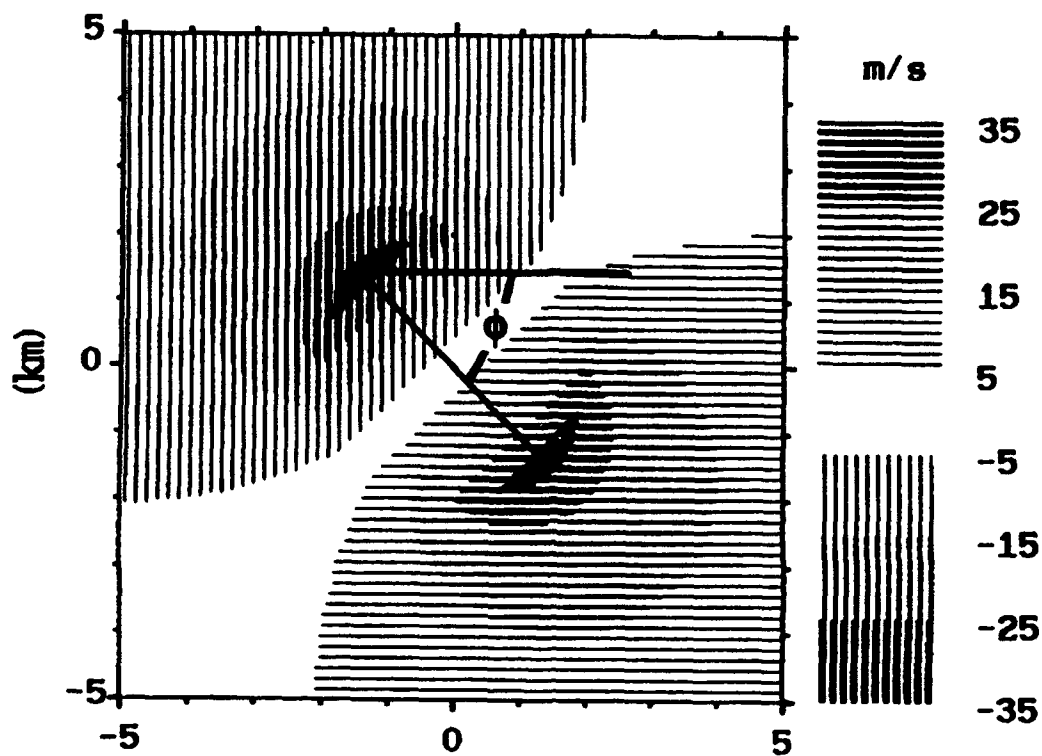


Figure 2. Theoretical Appearance, as Seen by Single-Doppler Radar, of a Circular Mesocyclone Containing Equal Magnitudes of Vorticity and Convergence. Contour levels are as indicated in Figure 1. The relative magnitudes of vorticity to convergence or divergence is indicated by the velocity peaks' orientation angle (ϕ) measured relative to the azimuthal direction. Here, ϕ equals -45° .

In the region of potential flow for rotation, u_x and u_y vary with distance from the vortex center according to Eq. (2). The rotational velocity decreases with increasing distance from the mesocyclone center and $\partial u_y/\partial x = \partial u_x/\partial y$. The derivatives are equal in both sign and magnitude at any point, the rate of change of each decreases with increasing distance, and the vector product for vorticity is everywhere equal to zero in the potential flow area.

It seems unlikely that vorticity should actually change abruptly from zero to a constant across the ring of maximum mesocyclone velocity. Regardless of the validity of assuming solid body rotation in the core, it is reasonable to assume that a transition zone of increasing cyclonic vorticity exists in the so-called "potential flow region". If the rate of change of rotational velocity in the potential flow region is decreased from that prescribed by the circular model potential flow Eq. (2), such a transition is provided (not shown).

The divergence field associated with inflow or outflow is analogous to the vorticity field of the circular model for rotation, that is, $\partial u_x/\partial x = \partial u_y/\partial y$. Therefore, divergence within the core is given by

$$\text{Divergence } (\nabla \cdot \vec{V}) = 2 \partial u_x/\partial x = 2 V_0 \sin(\phi)/R = 2 V_d/R. \quad (4)$$

The vorticity and divergence field for the circular mesocyclone example of Figure 2 is shown in Figure 3. Recall that in Figure 2, where $\phi = -45^\circ$, the magnitudes of vorticity and convergence inside the core are equal. The circular model is characterized by uniform vorticity and divergence (convergence in this case) associated with the core region. In the region described by potential flow, vorticity and divergence are both zero.

In summary, the circular mesocyclone model is characterized by uniform vorticity and divergence in the core region. The relative magnitudes of these quantities are determined by the orientation of the velocity peaks with respect to the radar (ϕ). From an observer's point of view, uniform divergence or vorticity in a single-Doppler velocity field is indicated by straight isodops (velocity contours), as seen in the core region of Figures 1b and 2. This is sometimes, but not always, a good approximation of what is seen in nature. Also, from Figures 1b and 2, it is obvious that the zero line (indicated by the non-shaded region) is always perpendicular to a line connecting the velocity peaks in the core. There is generally some deviation from this in single-Doppler observations. In the "potential flow" region, the circular model is perhaps less accurate than for the core. The impact of this for evaluating mesocyclone intensity is minimal because those evaluations concern only the core, where the concentration of energy is greatest.

3. NON-CIRCULAR ROTATION AND NON-SYMMETRICAL FLOWS

It has been recognized that mesocyclones do not always assume a circular, RCV-like flow pattern. Wood (1991), for example, examined the envelope of azimuthal gradients in the single-Doppler field and compared it to the envelope predicted by a circular flow⁹. His work documents several single-Doppler cases where the mesocyclone flow appears to deviate considerably from the circular mesocyclone model. The observed deviation is sometimes due to embedded vortices that confuse the issue. At other times the vortex appears singular but distorted in shape.

In the multiple-Doppler study by Brandes⁷ of the 1977 Del City, Oklahoma, mesocyclone, where the total horizontal wind field is more completely determined, the mesocyclone, as defined by a vorticity magnitude, is elongated. An example from this work will be discussed in Section 4.

Deviations from the circular mesocyclone model are sometimes obvious in even single-Doppler data. Distorted flows are seen most often at low levels but can extend to middle storm levels as well. It is not clear at this time what distortions exist at the upper reaches of a storm. The high elevation angles required for sampling these regions result in degraded horizontal resolution of the data and a stronger contribution by the vertical velocities to the radial component. Examples of highly distorted low level flows from the Del City mesocyclone are shown in Figures 4 and 5. The times selected are for volume scans beginning at 1826 and 1832. At 1840 the storm's first tornado occurred, classified as F2 on the Fujita scale¹⁰.

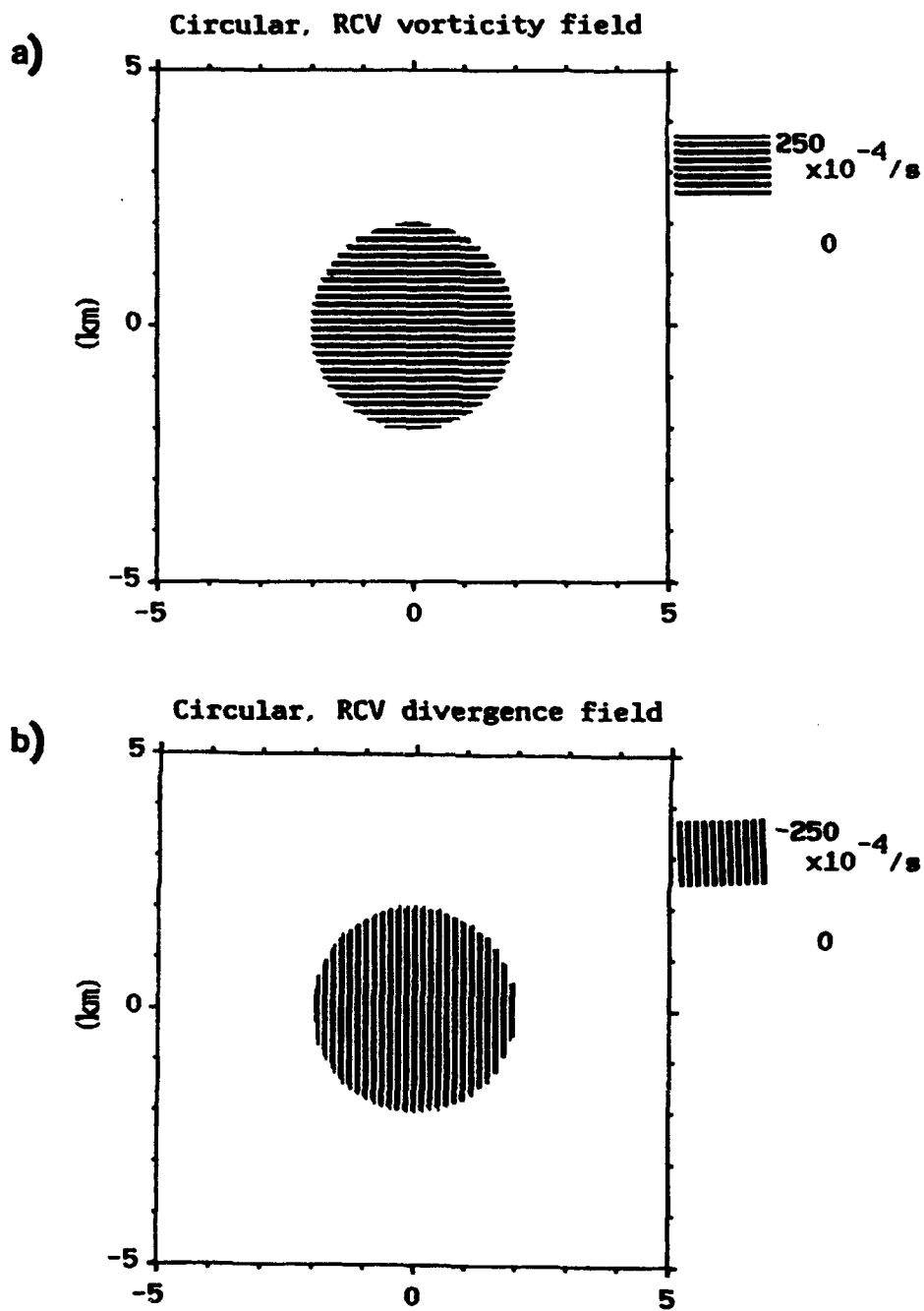


Figure 3. The Associated Vorticity and Divergence (convergence) Fields for a Circular RCV Flow Associated with the Example in Figure 2.

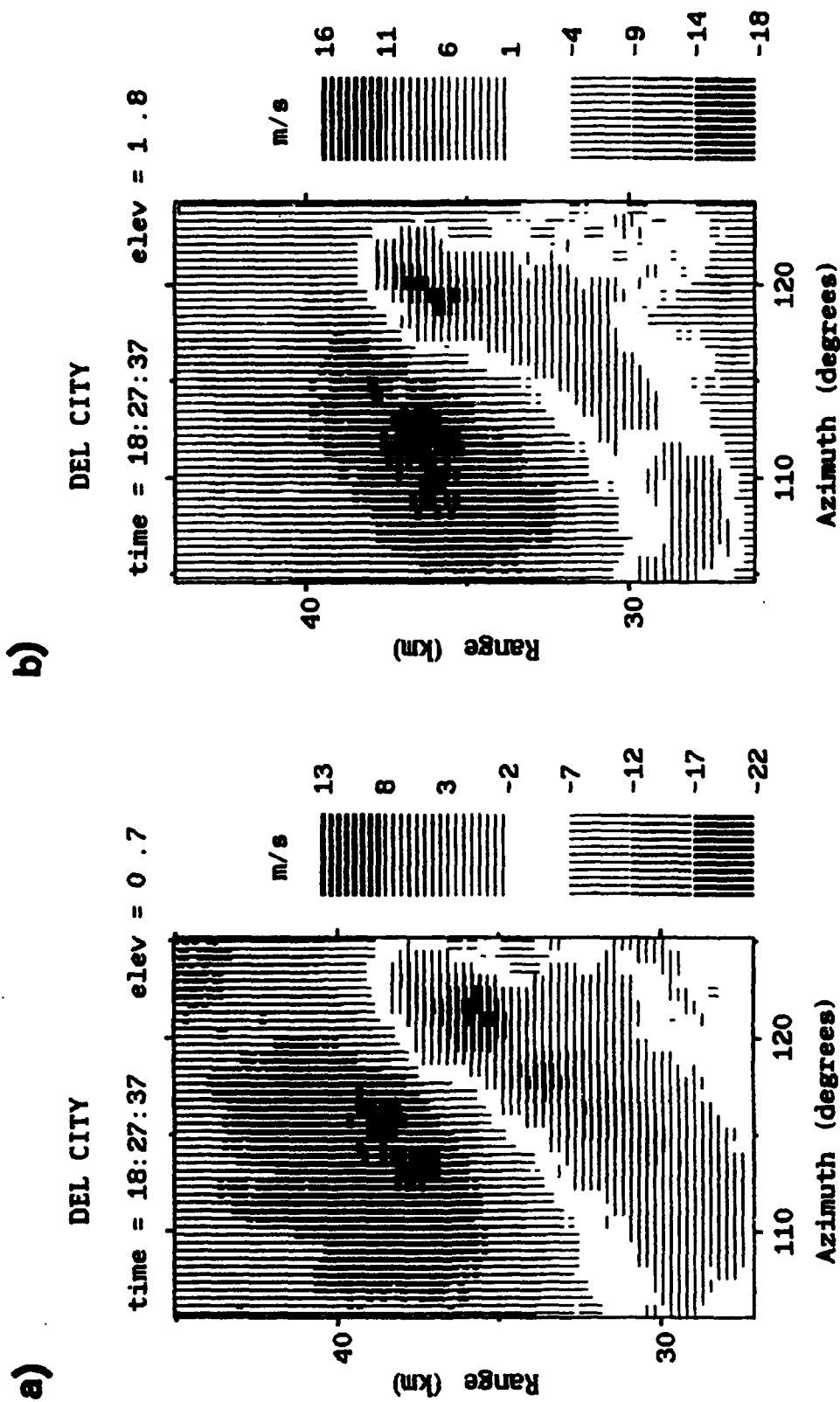
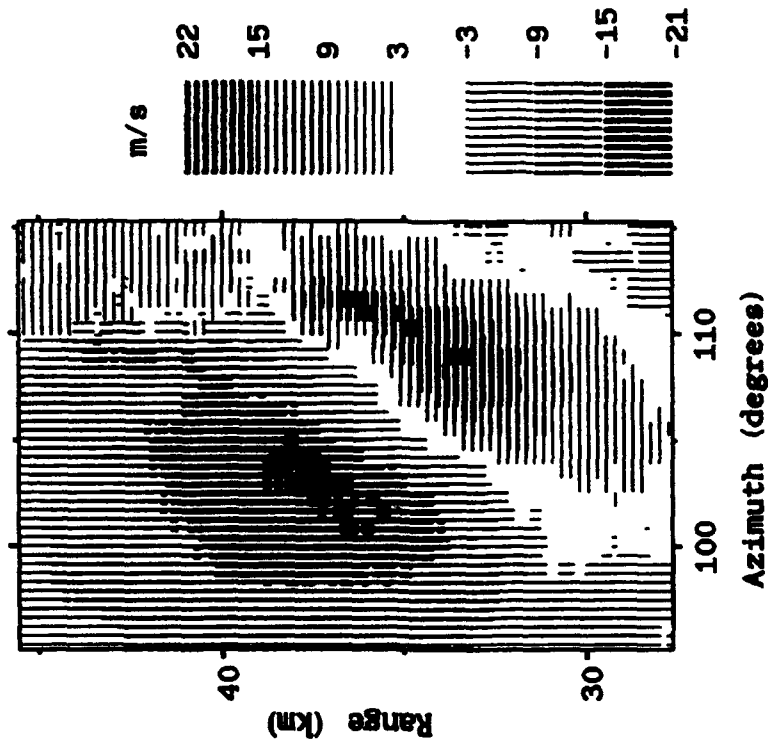


Figure 4. B-scan Format of the Del City, OK, Storm of 20 May 1977 at 1827 CST. Data as Collected From the National Severe Storms Laboratory 10 cm Doppler Radar Located in Norman, OK. Range and azimuth scaling are adjusted so they represent approximately equal distances. Contour levels are as indicated in Figure 1. a) The 0.7° elevation scan. b) The 1.8° elevation scan.

a)

DEL CITY

time = 18:32:39 elev = 0.8



b)

DEL CITY

time = 18:32:54 elev = 1.7

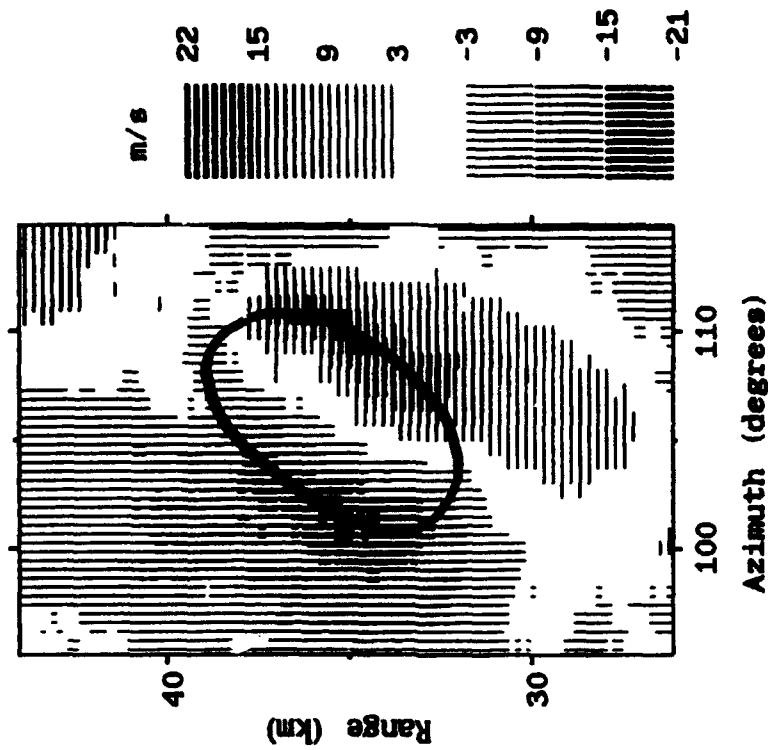


Figure 5. Same as Figure 4, but for the Radar Volume Beginning at 1832 CST. a) The 0.8° elevation scan. b) The 1.7° elevation scan. The thick solid line is an eyeball estimate of the core region.

The scaling presented in Figures 4 and 5 is nearly equal in the azimuthal and radial dimensions. Because of the range-azimuth displays, there is some distortion to the data. However, the mesocyclone is sufficiently far from the radar that the distortion attributable to the display is small compared to the natural distortion in the mesocyclone flow. There are several distinctive qualities to the examples. First, variations in the contouring are somewhat suggestive of the circular mesocyclone model; that is, there appear to be inner and outer flow regimes. Second, in contrast to the circular model, the line connecting the velocity peaks in the Del City example is not always perpendicular to the zero line (see Figures 4b and 5b for example). Finally, the envelope in the isodops separating the inner and outer flow regions appears to be approximately elliptical in shape. Figure 5b illustrates this elliptical shape.

A principal problem to solve in modeling the elliptical flow is the determination of reasonable kinematics constraints. As a starting point, the mesocyclone is examined from a two-dimensional (2-D) perspective, although it is in reality, a three-dimensional feature. Therefore, constraints can only be applied to the rotational aspect of the flow. For simplicity, the model is developed where vorticity is uniform inside the core. The affect of applying fields of uniform divergence is then examined. The process used for combining the features is simple; separate fields for rotation and inflow are generated; and then they are vectorially combined to generate the total two-dimensional flow field. This simple approach allows easy examination of important aspects of the model.

3.1 Rotation in an Elliptical Flow

The orientation of the Del City "ellipse" with respect to the radar is relatively unchanged with time (Figures 4 and 5). This means that we are not observing an elliptical pattern rotating about an axis, but rather an elliptical flow. Also, the changing position in space of the velocity peaks suggests an evolving vorticity and divergence field. It will be shown here that the general characteristics of the single-Doppler velocity field can be simulated with a simple two-dimensional (2-D) mesocyclone model.

Mesocyclone rotation is modeled by an ellipse with vertices ($\pm a$), covertices ($\pm b$), (as shown in Figure 6a), and thickness. Cross-sectional areas along a and b through which the flow travels are given by $A_a = a \Delta h$ and $A_b = b \Delta h$. Constant mass flux is assumed for the rotational flow such that

$$\rho A_a \bar{V}_a = \rho A_b \bar{V}_b, \quad (5)$$

where \bar{V}_a and \bar{V}_b are the average velocities through the cross sectional areas, and ρ is air density, held constant throughout the horizontal flow. For a rotational flow to satisfy Eq. (5), air traveling across the ellipse major axis (a) must experience an increase in angular speed (ω) to pass through the minor axis (b), so the angular speed at a is not the same as b ; $\omega_a \neq \omega_b$. If ω is held constant along any given radius arm of the ellipse, akin to the inner flow of the circular mesocyclone model, then ($\bar{V} = \omega a/2$) and ($\bar{V}_b = \omega b/2$). Therefore,

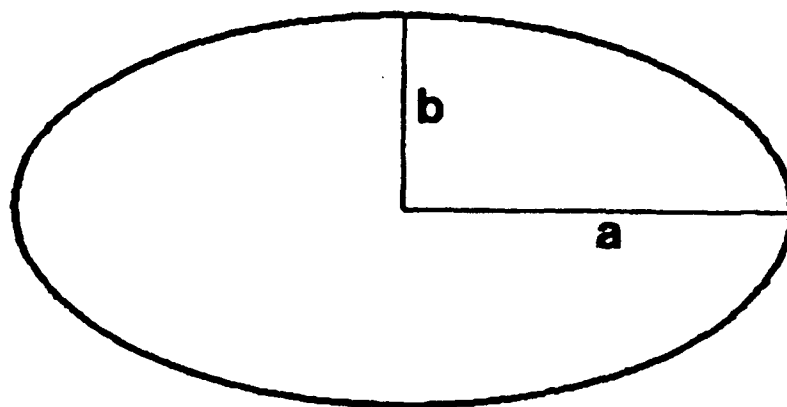
$$\rho a^2 \Delta h \omega_a/2 = \rho b^2 \Delta h \omega_b/2. \quad (6)$$

The peak rotational velocities along a and b are given by V_a and V_b . Therefore, $\omega_a = V_a/a$, $\omega_b = V_b/b$, and

$$a V_a = b V_b. \quad (7)$$

In a purely rotational flow, the wind is tangent to the ellipse surface, and the magnitude of the rotational velocity is just the component of the velocity that is normal to the ellipse radial arm. Along axes a and b the flow tangent to the ellipse is also normal to the radius arm, but for all radii in between, the rotational velocity is given by the velocity along the ellipse surface multiplied by $\sin(\alpha)$, where α is the obtuse angle between the radius arm of the ellipse and the tangent to the ellipse (Figure 6b). The angle α is given by $(90^\circ + \xi - \beta)$. ξ is the ellipse relative angle that varies

a)



b)

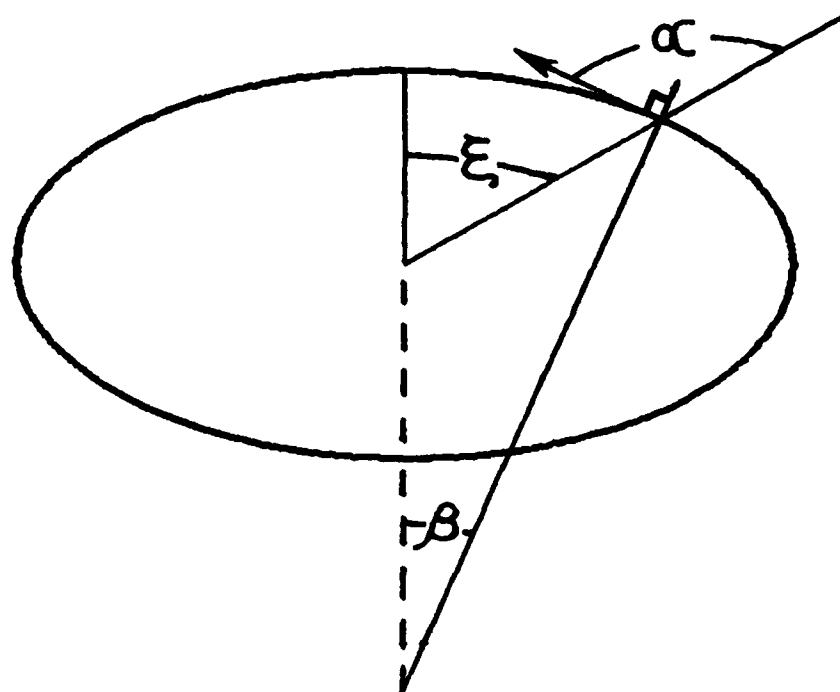


Figure 6. Elliptical Mesocyclone Model Setup. a) Horizontal view with major and minor ellipse radii given by a and b , respectively. b) Model reference angles, where $\alpha = 90^\circ + \xi - \beta$.

between 0° and 90° with 0° towards the ellipse "top" along the minor axis. β is the arctangent of the slope along the ellipse.

With an ellipse defined by $(x^2/a^2 + y^2/b^2 = 1)$, the slope along the curve is given by

$$\frac{dy}{dx} = \frac{-b x}{a^2 (1 - x^2/a^2)^{0.5}} \quad (8)$$

If the coordinate system is defined with ξ measured positively in a clockwise sense and $\xi = 0^\circ$ along the minor axis (b), then $(x = R\{\xi\} \sin(\xi))$, where $R\{\xi\}$ is the ellipse radius as a function of ξ . The parameter $R\{\xi\}$ is given by

$$R\{\xi\} = \left(\frac{a^2 b^2}{b^2 \sin^2(\xi) + a^2 \cos^2(\xi)} \right)^{0.5} \quad (9)$$

and the slope, dy/dx , can be represented as a function of ξ :

$$\frac{dy}{dx} = \frac{-b^2 \tan(\xi)}{a^2} \quad (10)$$

Therefore,

$$\alpha = 90^\circ + \xi - \tan^{-1} \left(\frac{dy}{dx} \right) \quad (11)$$

To maintain a constant mass flux within the ellipse,

$$R\{\xi\} V\{\xi\} \sin(\alpha) = R\{\xi\} V_r\{\xi\} = C_{mf} \quad (12)$$

where $V\{\xi\}$ is the velocity along the ellipse perimeter at $R\{\xi\}$ as a function of ξ , $V_r\{\xi\}$ is the rotational velocity, and C_{mf} is the mass flux constant defined by $(C_{mf} = bV_b = aV_a)$. Equation (12) describes the variation in radius and velocity along the ring of maximum velocity that separates the inner and outer flow regions. Within the core region, the rotational velocity varies by

$$v_r / r = V\{\xi\} \sin(\alpha) / R\{\xi\} = V_r\{\xi\} / R\{\xi\} = C_1\{\xi\}. \quad (13)$$

In the potential flow region, the rotational velocity varies by

$$v_r r = V\{\xi\} \sin(\alpha) R\{\xi\} = V_r\{\xi\} R\{\xi\} = C_2\{\xi\}. \quad (14)$$

These relationships are analogous to Eqs. (1) and (2) for the circular mesocyclone.

Examples of the elliptical mesocyclone model for purely cyclonic rotation, where the total velocity is directed along the ellipse, are given in Figure 7. Simulated is the velocity distribution that would be detected by single Doppler radar, with the radar located towards the bottom of the page. These examples are for an arbitrary eccentricity of 0.866, which corresponds to a *stretch factor* (S) of 2. Stretch factor is defined as the ratio of the ellipse major and minor axes (a/b). This means that that $S = 1$ for a circle and $S > 1$ for an ellipse.

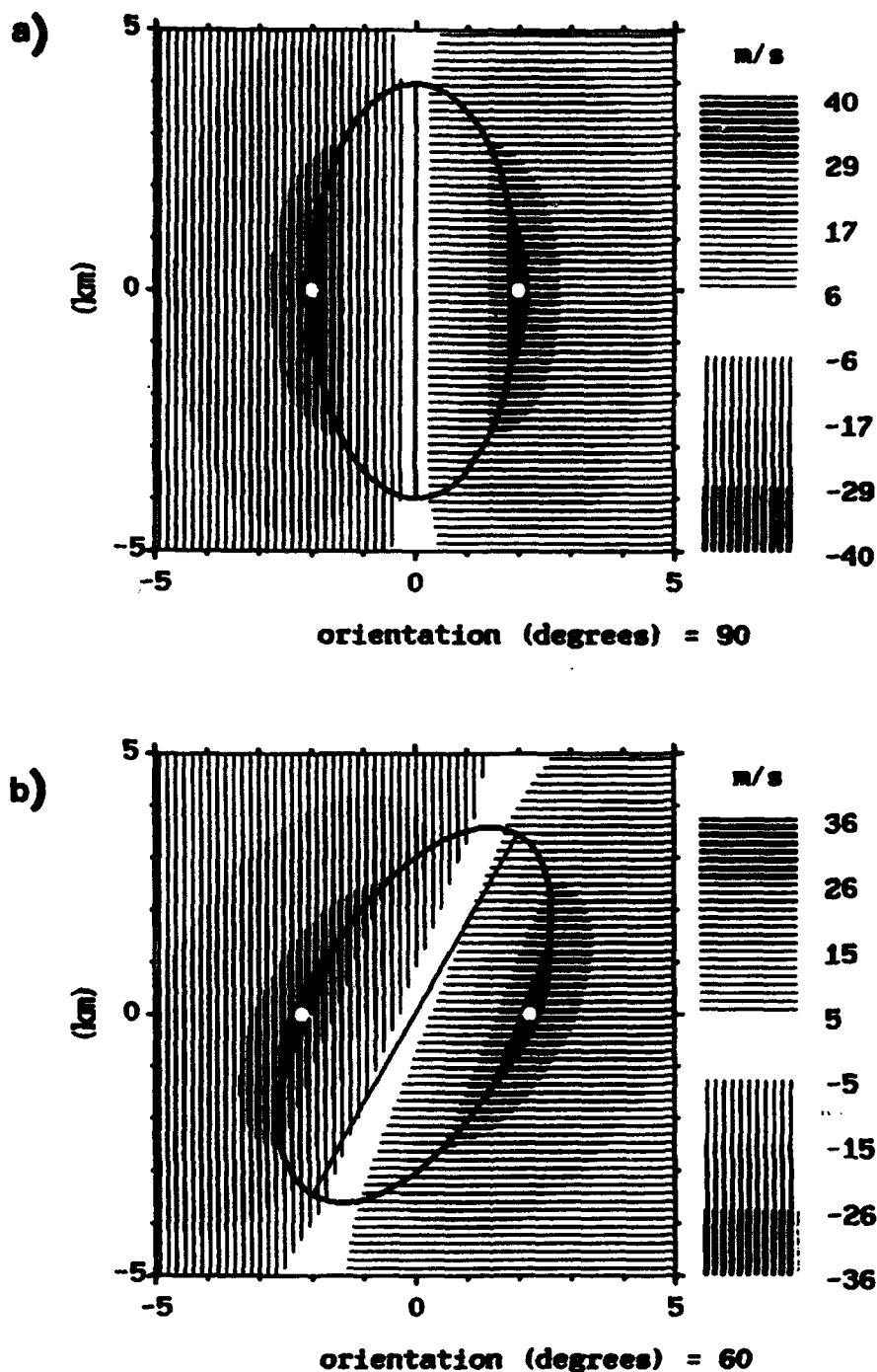


Figure 7. Examples of The Elliptical Mesocyclone Model for the Condition of Pure Rotation (that is divergence is everywhere equal to zero). The velocity distribution that would be detected by a single Doppler radar, located towards the bottom of the page, is shown. Contour levels are as indicated in Figure 1. White circles indicate the precise location of velocity maxima. Example shown is for an ellipse of axial stretch factor (S) = 2. Ellipse size, shape, and orientation relative to the radar are indicated by the thick solid line. The straight line bisecting the ellipse is oriented along the major axis. The examples, a,b,c, and d are for the same feature observed at a feature orientation angle (θ_f) of 90° , 60° , 30° , and 0° , respectively.

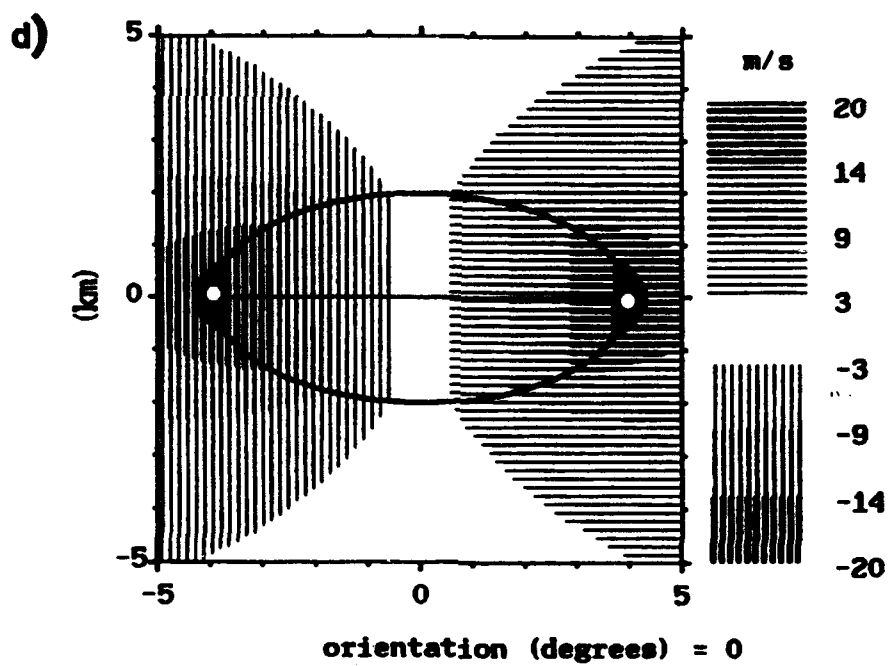
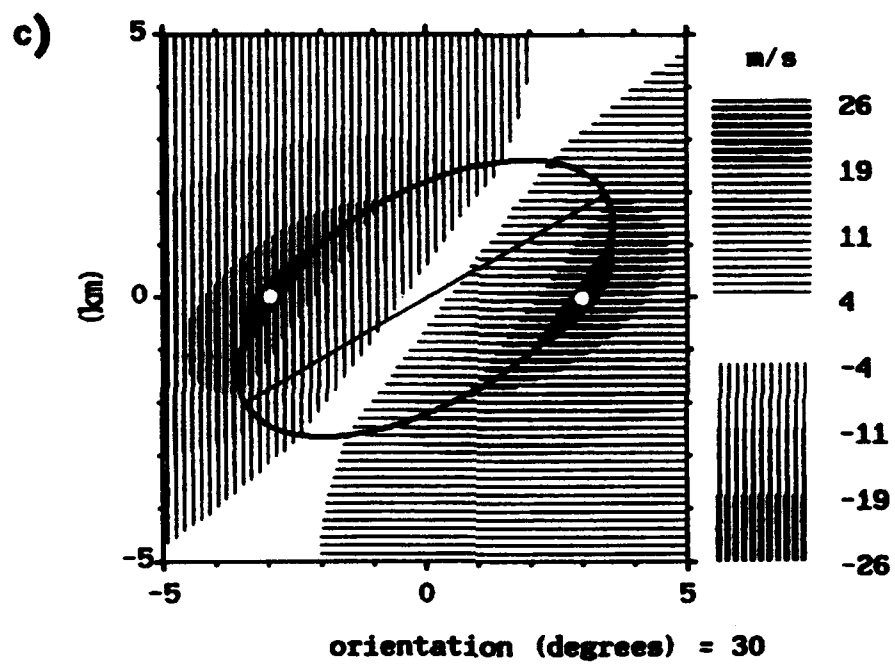


Figure 7. (Continued)

The examples shown in the figure represent the same theoretical elliptical mesocyclone at various orientations to the radar. The feature *orientation angle* (θ_f) refers to the orientation of the ellipse relative to the radar. θ_f equal to 0° means the minor axis is aligned with the radar beam, as in Figure 7d. Positive (negative) values of θ_f indicate counterclockwise (clockwise) rotation of a feature.

The figure indicates that for a pure rotation scenario, the velocity peaks are always in a line normal to the radar beam ($\phi = 0^\circ$), regardless of θ_f . However, the magnitude of the detected velocity peaks and the distance between them varies greatly as a function of the ellipse orientation θ_f . Figure 8 shows the effect on the apparent mesocyclone shear of θ_f and stretch factor S . Here the observed shear is normalized to the peak value, which corresponds to $\theta_f = 90^\circ$.

The potential impact of ellipse orientation to the radar increases with the stretch factor. With even a modest stretch factor of 1.25, the detected shear by single-Doppler radar will be only 64 percent of the true peak value when the radar is looking broadside at the ellipse ($\theta_f = 0^\circ$). For the examples of Figure 7, with $S = 2$, the detected shear may be only 25 percent of the peak. This has important implications for mesocyclone detection. The established criteria for mesocyclone identification by single-Doppler radar require the detection of "mesocyclonic shear" at several contiguous elevations¹¹ (JDOP Staff, 1979). In practice, mesocyclonic shear is defined as 0.005/s or greater across the relative inbound and outbound velocity peaks associated with the observed velocity couplet. Therefore, with the present mesocyclone detection criteria, the early detection of all mesocyclones and the detection of marginal mesocyclones with peak shear near 0.005/s depends on the feature orientation relative to the radar. If mesocyclone elongation and orientation are a function of the low level inflow, there will be preferential regions for mesocyclone detection within the radar scanning circle. If the Del City storm is representative of Oklahoma, then the locations for optimal shear detection should be NNW and SSE of the radar.

Figure 5b of the Del City examples is represented fairly well by the model. The Del City example has a stretch factor (S) of about 1.9 and a feature orientation angle (θ_f) of approximately 55° . A single-Doppler model simulation with these characteristics is displayed in Figure 9 along with the Del City observation. There is good general agreement between the two. Orientation of the velocity peaks with respect to the radar is very similar, and the "zero line", indicated by the white contour interval (non-shaded), has about the same orientation with respect to the peaks, although with Del City the contours between the velocity peaks are not entirely as straight as in the model. In both, it is easy to determine the ellipse outline through the contour inflections at the border between the inner core flow and the potential flow region.

The Del City example is at a height of 1.1 km, which is generally low for pure rotation in a mesocyclone. However, this height is at the lower bounds of where Brandes⁷ found non-divergent flows to exist for this particular mesocyclone.

3.2 Kinematics of the Model Rotational Flow

Vorticity and divergence fields of the model are determined for pure rotational flow. The parameters are determined using a simple point differencing formulation from a Cartesian grid. For pure rotation, divergence is, by definition, equal to zero in both the inner and outer flow regions of the ellipse. The vorticity field is more interesting and is shown in Figure 10. As with the circular flow, vorticity is uniform within the ellipse core region and is equal to the average of the radial shear along the major and minor axes.

The figure shows examples where the inner vorticity is held constant while the stretch factor (S) is varied between 3.0, 2.0, 1.5, and 1.0. In the outer region, the elliptical flow produces a pair of anticyclonic vorticity peaks located either side of the ellipse minor axis. The magnitude of this negative vorticity relative to the positive vorticity of the core region varies as a function of the eccentricity: the greater the stretch factor, the greater the relative anticyclonic component.

While the couplet of anticyclonic vorticity is a by-product of the model, does it have some validity in real world? The examples in Figure 7 are for a rotational wind field that varies according to a general potential flow in the

Observed shear as function of ellipse orientation

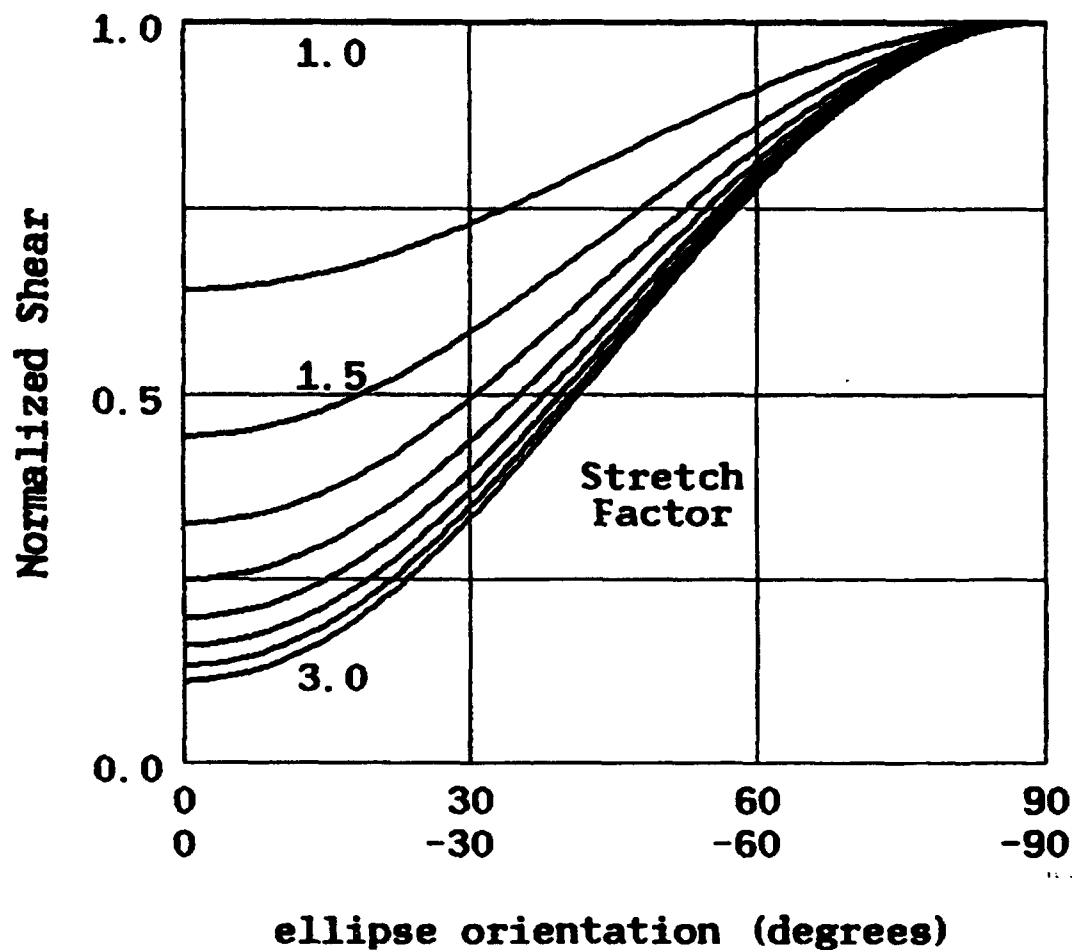


Figure 8. Detectable Shear, by Single-Doppler Radar, as a Function of the Mesocyclone (ellipse) Orientation with Respect to the Radar. The effect of stretch factor is examined with S varying from 1.0 (circular flow) to 3.0. Peak shear is detected when $\theta_r = 90^\circ$ for pure rotation (no divergence). Other shears within each category of S are normalized to this value.

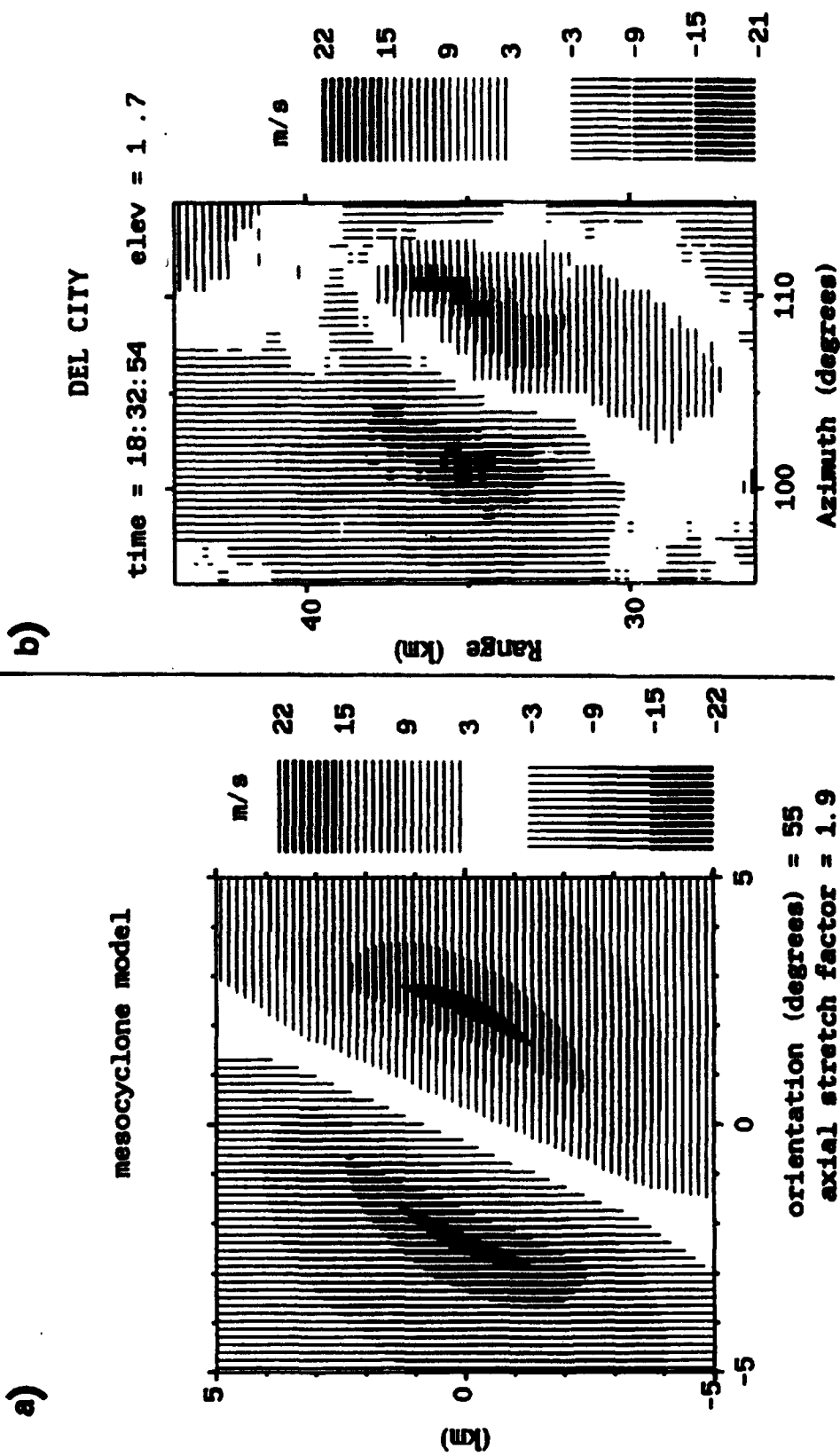


Figure 9. Comparison of the Model Output for Pure Rotation (shown in a) to a Real Life Example From the Del City Storm (shown in b). The model example approximates the Del City mesocyclone size and shape characteristics, and orientation to the radar. Presented scales of size are different. Contour levels are as indicated in Figure 1.

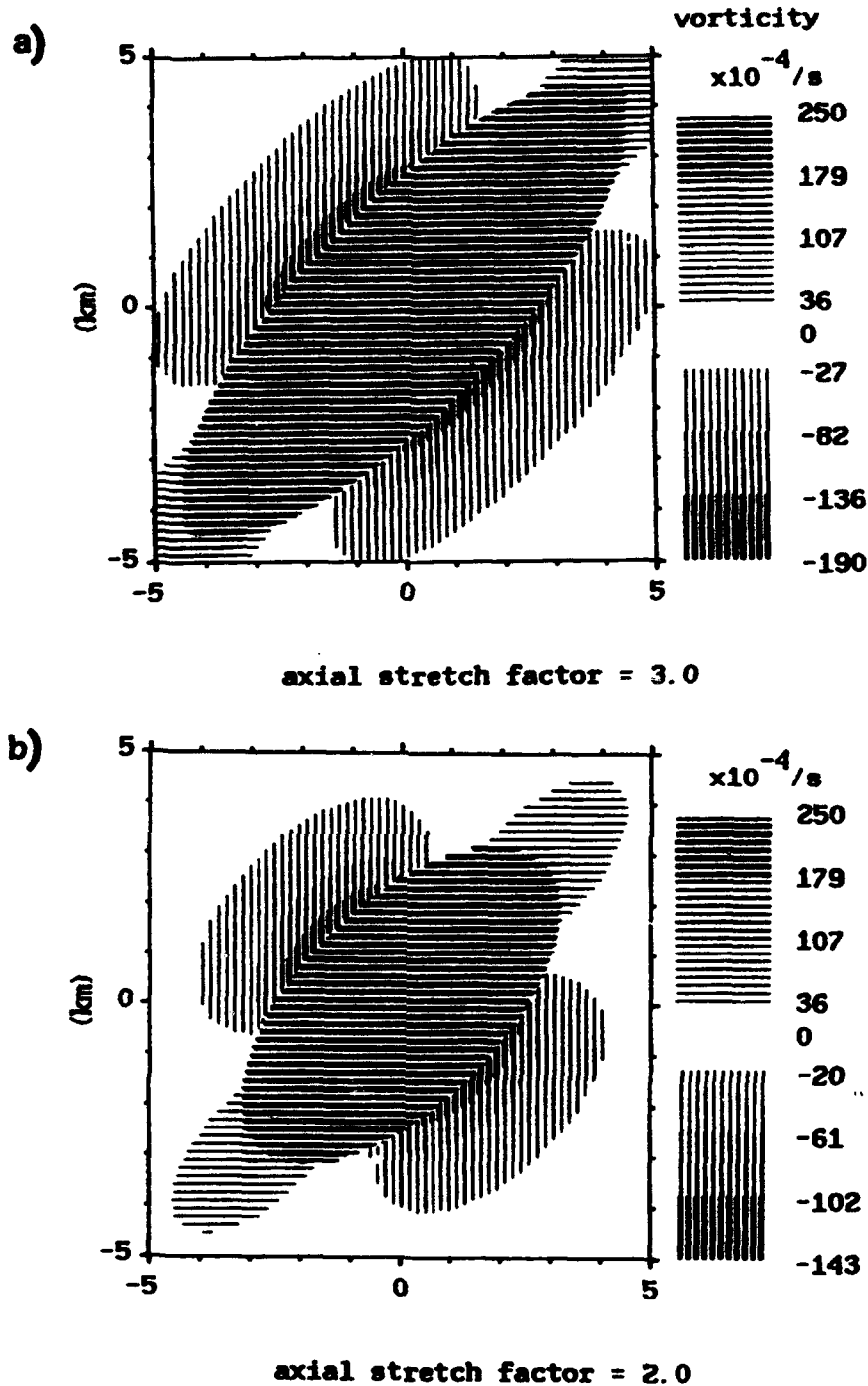
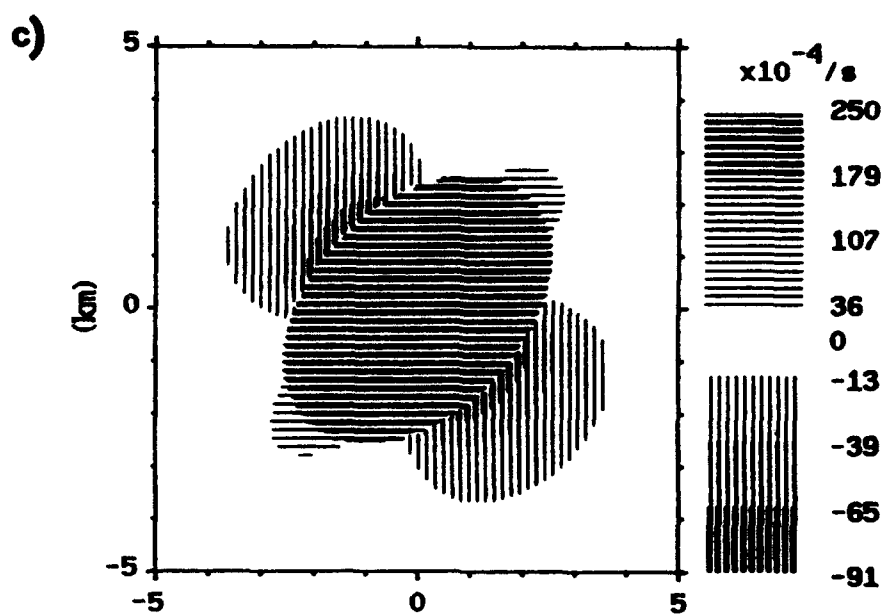
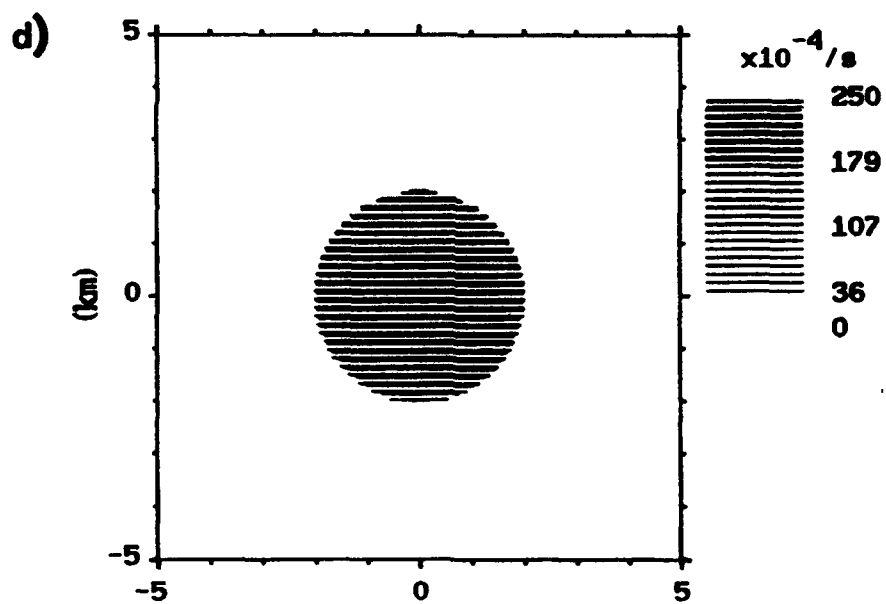


Figure 10. Presentations of the Vorticity Field for an Elliptical Mesocyclone Flow as a Function of the Stretch Factor. Peak velocities vary for each example to maintain the same vorticity magnitude in the core, $0.025/s$. The feature is presented at a orientation angle of $\theta_f = 45^\circ$, to show the vorticity contours as clearly as possible, but the vorticity field is, of course, not a function of the feature orientation to the radar. The example show how the peak in anticyclonic vorticity outside the core varies as a function of stretch factor; a) $S = 3.0$, b) $S = 2.0$, c) $S = 1.5$, d) $S = 1.0$.



axial stretch factor = 1.5



axial stretch factor = 1.0

Figure 10. (Continued)

mesocyclone outer flow region, as described in Eq. (14). While true potential flow is unlikely, it is interesting to examine how the flow in the outer region might be varied to eliminate the anticyclonic couplet entirely. Figure 11 shows how the velocity field, seen by single-Doppler radar, would have to vary to have no associated anticyclonic vorticity couplet. Such elongation of the velocity contours in the outer flow region is not seen in single-Doppler mesocyclone observations, and, therefore, the presence of negative vorticity pairs in a general elliptical mesocyclone flow is at least dynamically possible. This is interesting considering that some cyclonic tornadoes form in conjunction with an anticyclonic counterpart that is generally of lesser intensity. Whether such an anticyclonic vorticity zone serves as the source for amplification to tornado intensity is an important question, but beyond the present scope of this work.

3.3 Rotational Kinetic Energy

A convenient parameter for describing mesocyclone organization is Rotational Kinetic Energy RKE. While mesocyclone RKE is not especially effective for evaluating tornado potential¹² (Donaldson and Desrochers, 1990), it is a conservative quantity that may be useful for evaluating other types of severe weather, and is worthy of discussion here.

It is instructive to derive the equation for circular RKE. For circular mesocyclones it is convenient, and reasonable, to assume solid body rotation where vorticity is uniform in the core. Rotational kinetic energy is then simply $(I \omega^2/2)$, the product of moment of inertia (I) and angular velocity (ω). For a solid disk, $(I = m R^2/2)$, the product of the mesocyclone mass (m) and radius (R) of the core. Mass is given by $(\rho \Delta h \pi R^2)$. Angular speed (ω) is given by V_r/R . Rotational kinetic energy for a circular mesocyclone is represented by:

$$RKE_{\text{circle}} = m V_r^2 / 4 = \rho \Delta h \pi R^2 V_r^2 / 4 \quad (15)$$

The identical solution can be obtained by integrating the kinetic energy of a sector around the entire mesocyclone circle. It is necessary to take this approach for an elliptical mesocyclone because the flow cannot be described as solid body, although the vorticity field inside the core may be uniform. Also, an elliptical flow does not have a moment of inertia since the elliptical shape is not rotating around itself, but rather the flow is following a relatively steady elliptical shape. We begin with the rotational kinetic energy of an ellipse sector, η radians wide,

$$RKE_s = m_s (V_r @_{cm} \{\xi\})^2 / 2 \quad (16)$$

where $V_r @_{cm} \{\xi\}$ is the rotational velocity at the sector center of mass as a function of the ellipse relative angle ξ . The mass of a sector is given by $m_s = \rho \Delta h A_s$. The area of a sector is given by $(A_s = R\{\xi\}^2 d\eta/2 = R_{cm} \{\xi\}^2 d\eta)$, where $d\eta$ is the sector angular width, assumed small, and $R_{cm} \{\xi\}$ is the radius to the sector center of mass. The velocity along the ellipse at $R_{cm} \{\xi\}$ is $V_{cm} \{\xi\}$ and is given by $(V_{cm} \{\xi\} = \omega \{\xi\} R_{cm} \{\xi\} = V \{\xi\} R_{cm} \{\xi\} / R \{\xi\})$. Since the rotational velocity is a function of α : $(V_r @_{cm} \{\xi\} = V_{cm} \{\xi\} \sin(\alpha) = V \{\xi\} \sin(\alpha) R_{cm} \{\xi\} / R \{\xi\})$. From Eq. (12), $(V \{\xi\} \sin(\alpha) = a V_a / R \{\xi\})$, and substituting for $R_{cm} \{\xi\}$, the rotational kinetic energy for an elliptic sector is given by

$$RKE_s = \rho \Delta h a^2 (V_a)^2 d\eta / 8. \quad (17)$$

Integration of η from zero to 2π to obtain the total ellipse rotational kinetic energy yields:

$$RKE_{\text{ellipse}} = \rho \Delta h a^2 (V_a)^2 \pi / 4 = m_e a (V_a)^2 / 4b \quad (18)$$

where the ellipse mass (m_e) = $\rho \Delta h \pi a b$. For a circle, where $a = b$, Eq. (18) reduces to Eq. (15).

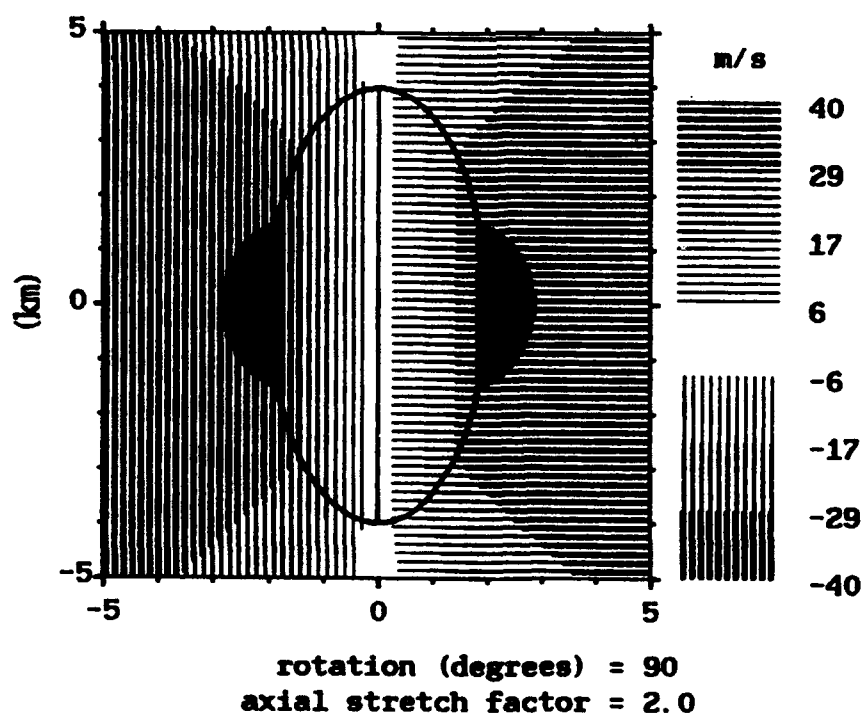
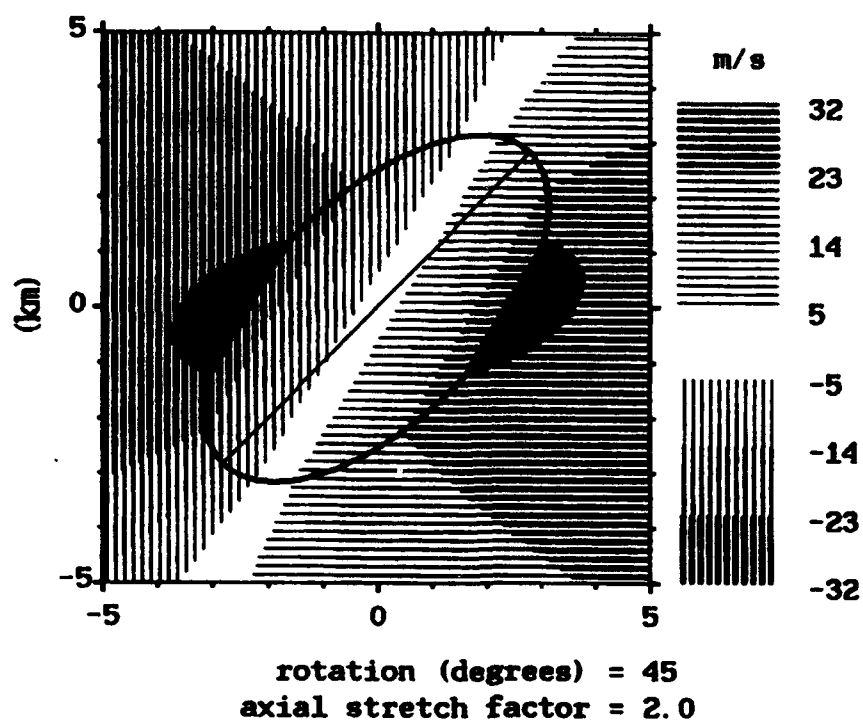


Figure 11. An Example of How the Velocity Field in the Potential Flow Area of an Elliptically-shaped Mesocyclone Would Have to Vary to Have Zero Anticyclonic Vorticity. Contour levels are as indicated in Figure 1.

ellipse. Therefore, ellipse RKE can be determined without knowledge of the eccentricity, ellipse orientation to the radar, or the magnitude of V_a or V_b . The single-Doppler velocity peaks can be applied to the relationship for a circular mesocyclone Eq. (15) to yield the RKE of the ellipse, regardless of the eccentricity. Mesocyclone rotational kinetic energy is therefore a conservative quantity for detection. Unfortunately, in our own investigations, RKE has not been found to be of significant value for evaluating the mesocyclone for hail or tornado potential.^{13,12}

3.4 Excess Rotational Kinetic Energy

Donaldson and Desrochers¹⁴ present the concept of Excess Rotational Kinetic Energy (ERKE), which has subsequently been shown to offer promise for hail and especially tornado prediction (for example, Desrochers and Donaldson,⁶). From their work, ERKE for a circle is given by

$$ERKE_{\text{circle}} = \rho \Delta h \pi R^2 (V_r - R S_m)^2 / 4 \quad (19)$$

where S_m is an arbitrary shear threshold that defines mesocyclone rotation, nominally 0.005/s (after Donaldson²). ERKE is defined to exist only for $(V_r - R S_m) > 0$. ERKE is simply the rotational kinetic energy in excess of what would be needed to sustain mesocyclone rotation. The idea of ERKE is to distinguish large, well-organized, and swiftly rotating features that may present a severe weather threat from features that may have greater RKE but are benign.

ERKE for an ellipse can be determined in an analogous manner to RKE_{ellipse} . The ERKE of an ellipse sector is represented by

$$ERKE_s = \rho R \{\xi\}^2 (V\{\xi\} \sin(\alpha) - R\{\xi\} S_m)^2 d\eta / 8. \quad (20)$$

Here, in analogy with the circular flow, ERKE exists for $(V\{\xi\} \sin(\alpha) > R\{\xi\} S_m)$. Since the radial shear varies according to the ellipse relative angle (ξ), it is possible that radial shear satisfies S_m for only a sector of the ellipse. Substituting Eq. (9) for $R\{\xi\}$ into the inequality and solving for ξ , the maximum ellipse relative angle for integrating Eq. (20) for ERKE in the first quadrant of the ellipse is

$$\xi_{\text{max}} = \cos^{-1} \left(\frac{b^2 [(a^2 S_m / b V_b) - 1]}{a^2 - b^2} \right) \quad (21)$$

Expansion and integration of Eq. (20) for each ellipse quadrant yields the ERKE for an ellipse:

$$ERKE_{\text{ellipse}} = \rho/2 \int_{\xi=0^\circ}^{\xi=\xi_{\text{max}}} (a^2 V_a^2 - 2 a V_a S_m R\{\xi\}^2 + R\{\xi\}^4 S_m^2) d\xi. \quad (22)$$

Figure 12 shows Eq. (22) evaluated using Simpson's rule and normalized by the corresponding value of RKE. Here, the stretch factor (S) is varied between 1.0 and 3.0, and the shear threshold S_m is varied between 0.001/s and 0.009/s. RKE_{ellipse} is kept constant for the calculations and is determined for a climatological mature mesocyclone of 2.75 km radius and 23.3 m/s rotational velocity (after Burgess et al.¹⁵).

With RKE_{ellipse} kept constant as a reference, ERKE decreases as the mesocyclone becomes more elongated, because the average shear decreases. The change with S_m is a function of the products $(a V_a)$ and $(b V_b)$, which are proportional to RKE. For a low shear threshold ($S_m = 0.001/s$), ERKE decreases by 26 percent between $S=1$ and $S=3$. At progressively higher shear thresholds, the relative reduction in ERKE increases. For example, at $S_m = 0.005/s$ ERKE is diminished by about 72 percent between $S=1$ and $S=3$.

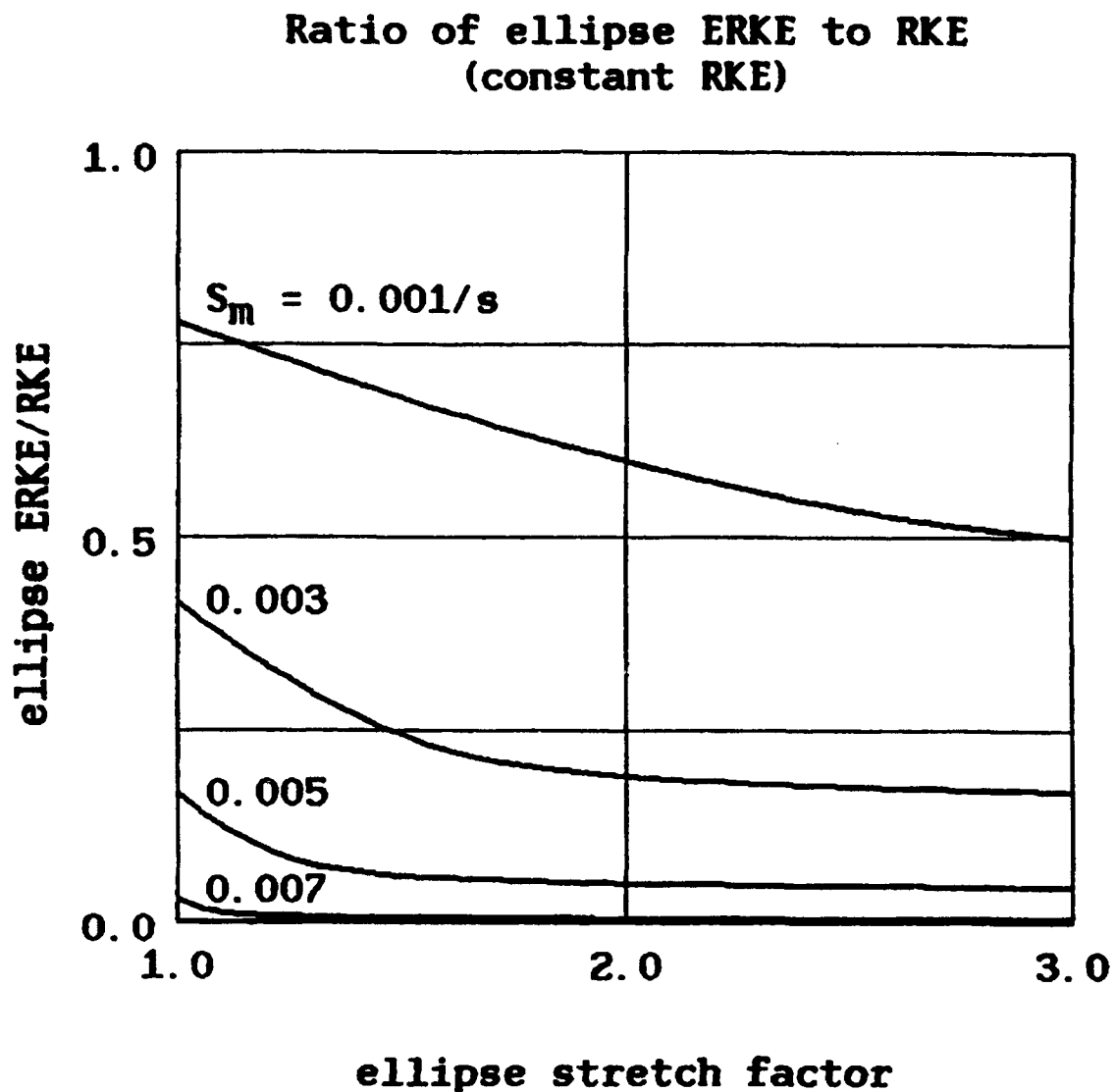


Figure 12. Variation of ERKE as a Function of Ellipse Stretch Factor (S) and ERKE Shear Threshold (S_m). Values are normalized by RKE calculated for $b = 2750$ m and $V_b = 23.3$ m/s, climatological values of an average mature mesocyclone (from Burgess et al.¹⁶).

Another way to examine ERKE is to compare it to vorticity. Figure 13 shows ERKE variation with vorticity and stretch factor. Here, ERKE at $S_m = 0.005/s$ is calculated for various vorticity levels and is normalized to the ERKE value at $S = 3$. For any given magnitude of mesocyclonic vorticity within the core region, ERKE increases as a feature becomes more elongated. The relative change of ERKE decreases with increasing vorticity.

While the increase in ERKE with feature elongation at constant vorticity is notable, it would not be necessarily correct to infer that ERKE would indicate a significant alteration in analysis, that is in storm strength or structure, based solely on elongation. In fact, the variation in ERKE with elongation is small compared to the variation with vorticity. The Del City example of Figure 5b is an appropriate case to make this point. The time of this particular scan was only 5 min. before the first F2 tornado. Vorticity here is estimated at $0.02/s$, and with $S = 1.9$, the mesocyclone was significantly elongated. Comparing the ERKE of this feature to the ERKE of a more elongated feature at a lesser vorticity, and to a less elongated feature at a higher vorticity gives an indication of the importance of vorticity in ERKE. ERKE of the Del City case is roughly 17 times greater in magnitude than ERKE for a feature of one-half the vorticity ($0.01/s$) and $S = 3$. Experience indicates that such a marginal vorticity case would not be expected to produce significant tornadoes (for example, see Desrochers and Donaldson⁶). Compare this to a mesocyclone of twice the vorticity of the Del City mesocyclone. ERKE for a feature of $S = 1$, a circular case, and vorticity $0.04/s$, is roughly 4 times that of Del City. This is in the range of what is observed for violent tornado producing storms. For each doubling in vorticity magnitude there is nearly an order of magnitude increase in ERKE, which, except for very marginal mesocyclones, is greater than the change attributable to eccentricity. This assumes that $S = 3$ is a safe upper bound for eccentricity. In summary, vorticity contributes more to the variation in ERKE than eccentricity. At the marginal mesocyclone vorticity level, eccentricity is perhaps of little significance because it can not contribute to significant values of ERKE. At increasingly larger vorticity values, where the absolute magnitudes of ERKE are already significant, it is speculated that increased eccentricity may add to the apparent overall severity of the mesocyclone.

The investigation of ERKE in mesocyclones has to date assumed that the mesocyclone flow is circular (for example, Donaldson and Desrochers¹²). Given the considerable variability in the apparent size and rotational velocity of an elliptical mesocyclone, it is interesting to ask for what feature orientation a "circular" assumption would be accurate. In other words, at what orientation of the ellipse, relative to the radar, will the observed velocity peaks be of such magnitude and azimuthal separation that the Excess Rotational Kinetic Energy (ERKE) of the ellipse can be derived under the assumption that the peaks are associated with a circular flow?

Figure 14 shows the variation of "apparent" ERKE for an elliptical flow where the vorticity of the core and the shear threshold (S_m) are kept constant. Ellipses of various stretch factors are examined and viewed from different orientations. The vorticity magnitude $0.007/s$ has been selected to be that for climatological mature mesocyclones. The shear threshold is arbitrarily set at $0.005/s$. The velocity field is one of pure rotation. ERKE is determined assuming the radar observed velocity peaks are associated with a circular feature. These values are then normalized by the true ERKE of the feature.

While the results correspond to a climatological feature, the generalities revealed are important. ERKE estimation errors will be minimized when a feature is oriented about $\pm 45^\circ$ to the radar beam. For orientations at larger angles, ERKE may be overestimated by a factor of 2 or more as the maximum velocities along the ellipse minor axes are detected. At orientations less than 45° ERKE will be underestimated, so severely that a severe mesocyclone may appear to have zero ERKE. The amount of over- or underestimation will increase as a feature becomes more elongated. Even with modest eccentricity, the errors can be considerable. With a stretch factor of $S = 1.2$, ERKE estimation can be off by as much as 50 percent if the eccentricity is not known.

4. DIVERGENCE SCENARIOS FOR ELLIPTICAL FLOW

The divergence field for a circular flow has been discussed in Section 2. In this section, a few possible divergence scenarios for an elliptical flow are examined.

Variation of ERKE with vorticity and ellipse stretch factor

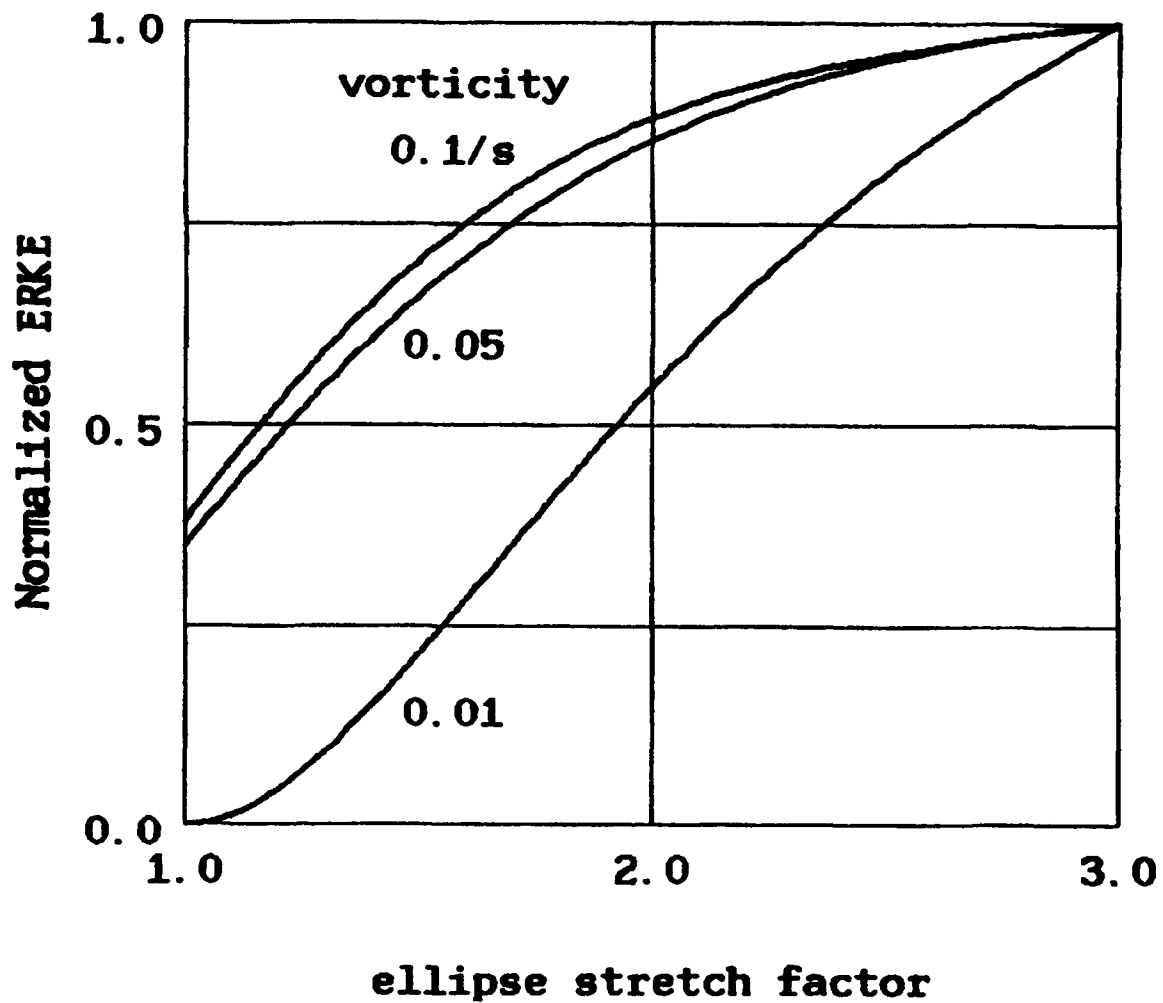


Figure 13. Variation of ERKE with Feature Eccentricity and Vorticity. Values of ERKE for each given vorticity level are normalized to the ERKE at a stretch factor of 3.0.

Ratio of circle ERKE to ellipse ERKE (constant vorticity)

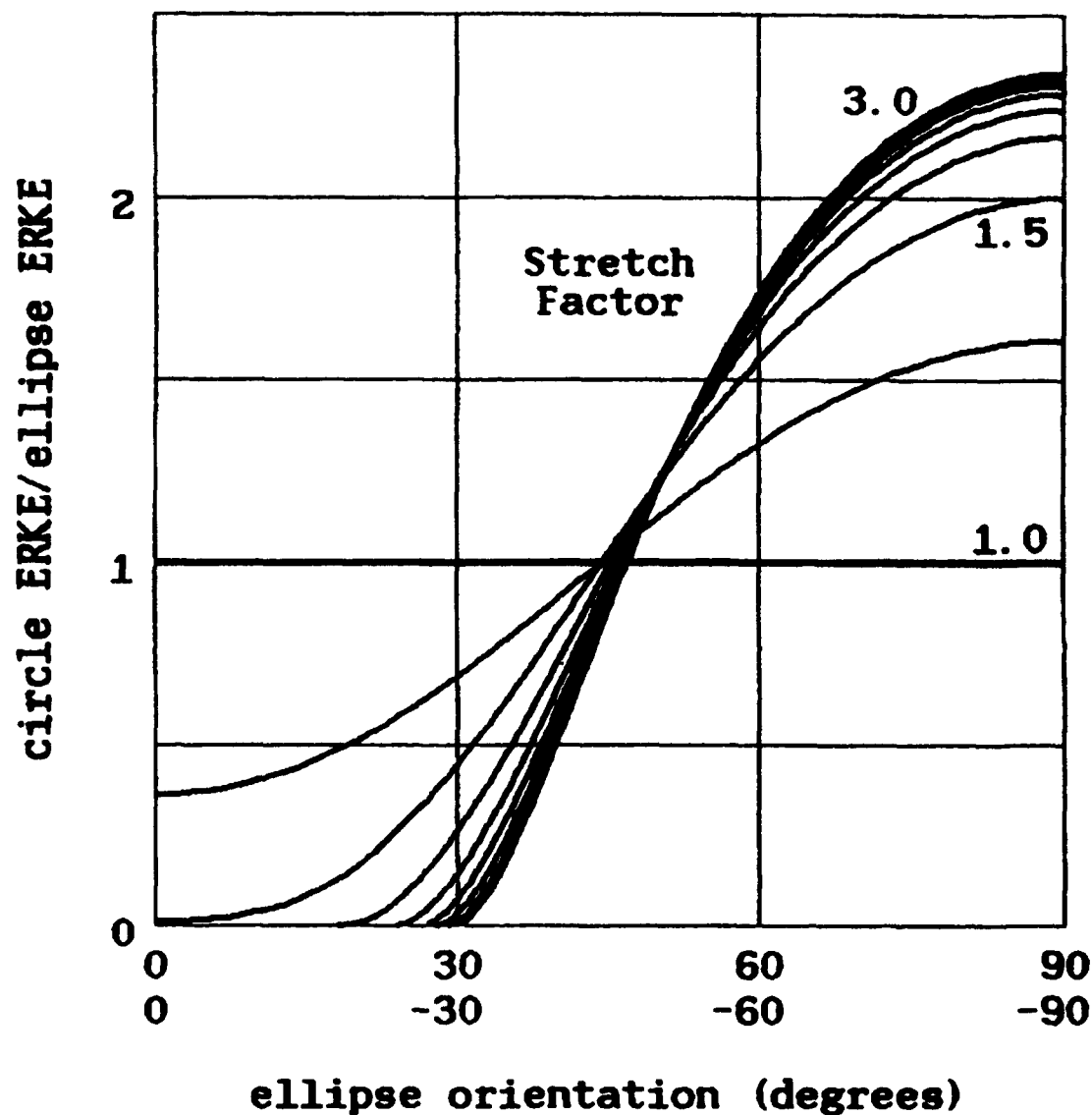


Figure 14. The Ratio of Circle ERKE to the True Ellipse ERKE as a Function of Stretch Factor (S) and Feature Orientation (θ_f). The intent is to illustrate potential errors in ERKE estimation by application of the old, circular mesocyclone model. Circle ERKE is determined from the single-Doppler mesocyclone observation, interpreted to be associated with a circular flow, regardless of how elliptical the true flow actually is. Vorticity is held constant for these calculations.

4.1 Uniform Divergence

A logical starting point is to simply reapply the mesocyclone model for divergence, such that flow is directed normal to, instead of along, the ellipse. Namely, $(R\{\xi\} V\{\xi\} \sin(\alpha) = R\{\xi\} V_d\{\xi\} = a V_a)$, where $V_d\{\xi\}$ is the divergent component of the velocity. A change in the direction of flow in this manner results in a flow field that has zero vorticity everywhere, and uniform divergence in the core region. Mesocyclone-like signatures in the Doppler field are not observed for purely convergent signatures, but signatures indicative of a purely divergent flow are sometimes seen at the upper reaches of a storm. A model example of the divergence field is shown in Figure 15, which is analogous to the model vorticity field (Figure 10b). Uniform divergence exists in the mesocyclone core region and extends into the potential flow region along the major axis. Along the minor axis, in the potential flow region, a divergence couplet of opposite sign to that of the core region exists.

An example of the single-Doppler appearance of the velocity field associated with the divergence field of Figure 15 is shown in Figure 16 at various radar-relative ellipse orientation angles. These examples are meant to represent upper storm outflow, as can be noted by the signs of the velocity contours. The flow is characterized by opposing velocity peaks oriented in the radial direction, ($\phi = 90^\circ$). Straight isodops in the core region mean uniform divergence exists there. Although the magnitudes of the peak velocities change as the ellipse is rotated with respect to the radar, the orientation of the peaks remains the same, as was also observed for pure rotation (Figure 8). It is interesting to see in Figure 15, that in a general divergent flow there is a convergence couplet in the potential flow region. This couplet is located along the direction of the minor axis where the outflow velocity is maximum. This result is produced by the assumption that the velocity magnitude strictly adheres to a potential flow rate of change, as in Eq. (14), which may not be realistic.

4.2 Uniform Convergence and Rotation

At most elevations through a mesocyclone, the flow field is comprised of a combination of divergence and vorticity. Here we examine low level inflow. Figure 17 presents single-Doppler views when the magnitude of convergence in the core region is equal to that of vorticity. This is shown for an arbitrary stretch factor (S) of 2.

The white dots in the figure indicate the location of the maximum radar-relative velocities. The orientation of the velocity peaks relative to the radar does not change if the feature is observed from different angles. Therefore, when divergence and vorticity are uniform within the core, as in these examples, the ratio of divergence to vorticity is a function of the velocity peaks' orientation angle (ϕ):

$$\frac{\text{Divergence}}{\text{Vorticity}} = \tan(\phi), \quad (23)$$

as is also true for the circular model (Section 2). This is a very useful quality, although the eccentricity must be known to determine the absolute magnitudes of divergence and vorticity.

Figure 5a, presented again for convenience in Figure 18b, shows an example from Del City where the elliptical mesocyclone core appears to be comprised of a combination of rotation and convergence. A velocity peak orientation angle ϕ of 31° indicates a divergence/vorticity ratio of -0.6. This relative magnitude of convergence in the flow is consistent with a 0.5 km height.

The model simulation (Figure 18a) compares well with the real-life example. The "zero line" of both, and the orientation of the velocity peaks, are similar. The relative straightness of the velocity contours within the core region of the Del City example would suggest that both convergence and vorticity are nearly uniform within the core. Velocity contours of the "potential flow" region do not agree as well. For one thing, there appears to be a change in the potential

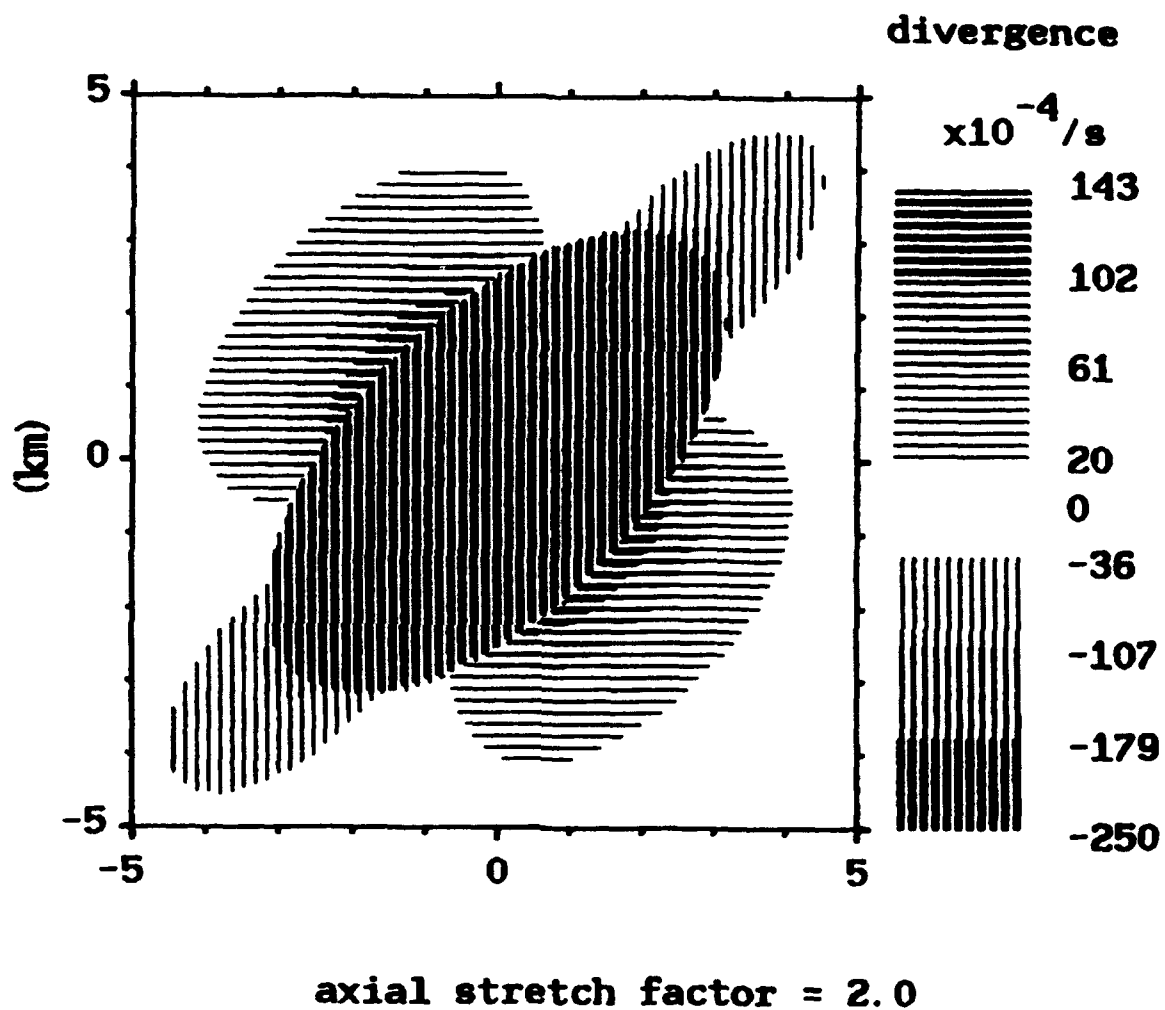


Figure 15. Example of the Divergence Field Produced by the Elliptical Mesocyclone Model. Divergence is uniform within the core. The divergence field is independent of the feature orientation presented. Divergence for a stretch factor of 2 is shown.

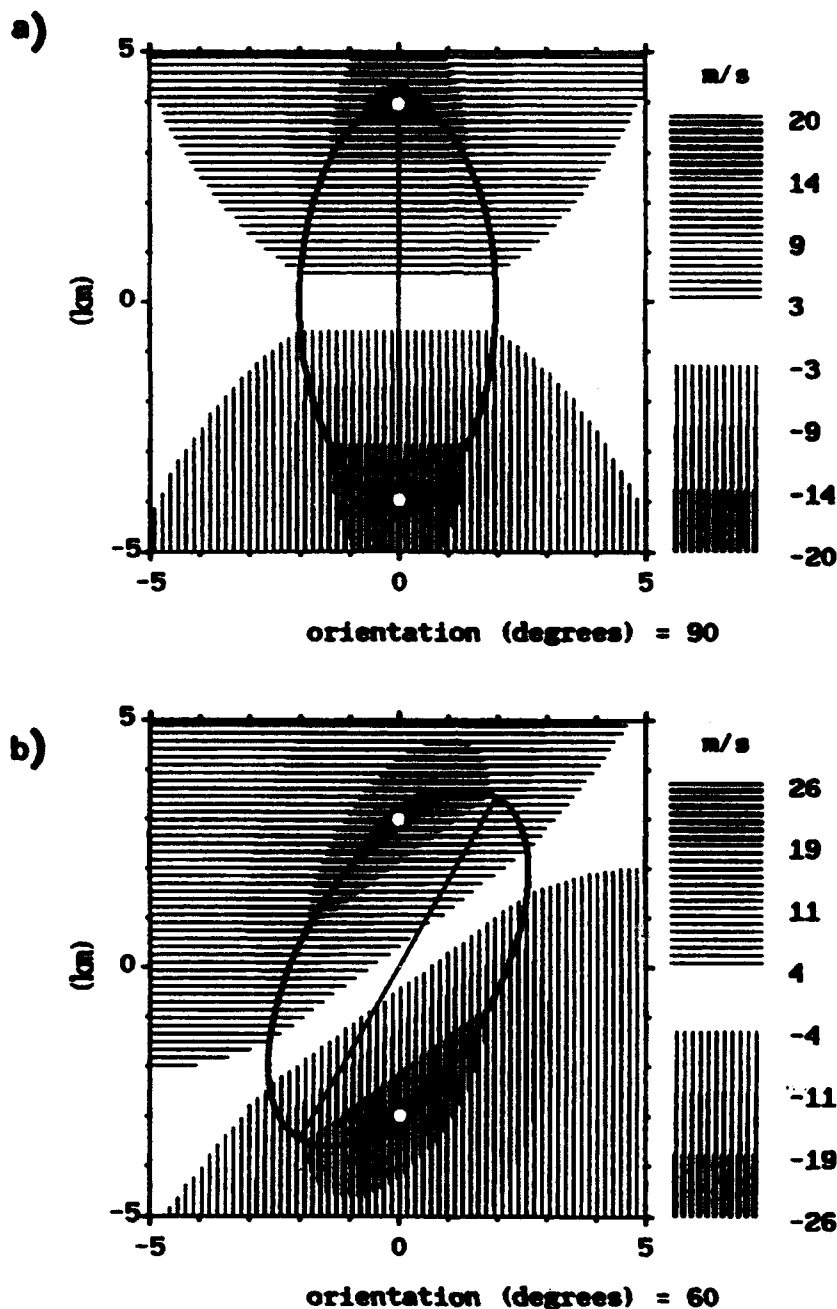


Figure 16. Examples of the Elliptical Mesocyclone Model for Pure Divergence. Within the core, the velocity field corresponds to uniform divergence. Outside the core, velocity tapers off according to a standard potential flow. The viewpoint is that of a single-Doppler radar, located towards the bottom of the page. Contour levels are as indicated in Figure 1. White circles indicate the precise locations of velocity maxima. Example shown is for an ellipse of stretch factor (S) = 2. Ellipse size, shape, and orientation relative to the radar are indicated by the thick solid line. The straight line bisecting the ellipse is along the major axis. The examples, a,b,c, and d are for the same feature observed at a feature orientation angle (θ_f) of 90, 60, 30, and 0°, respectively.

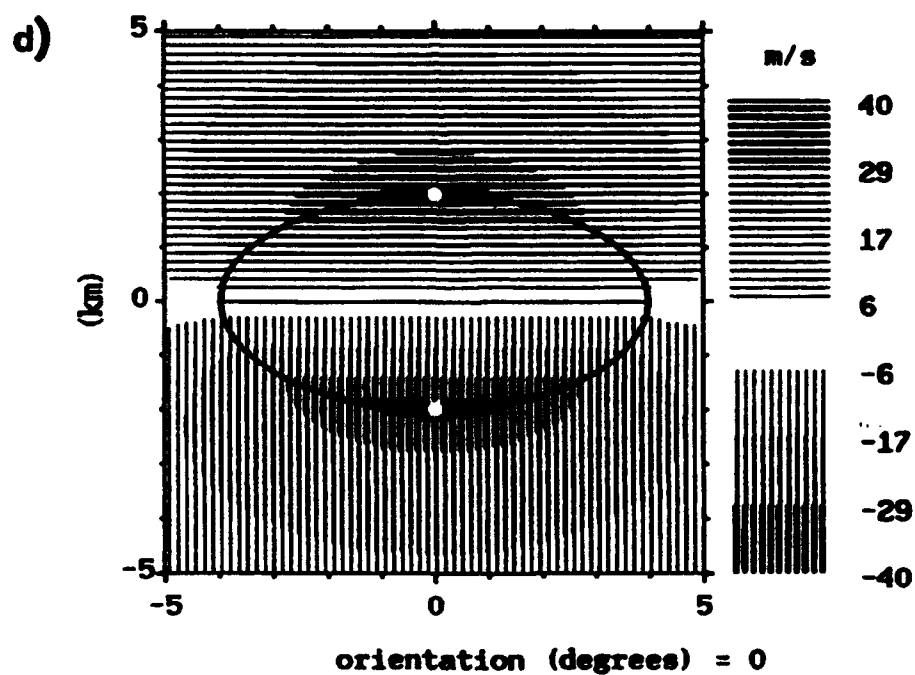
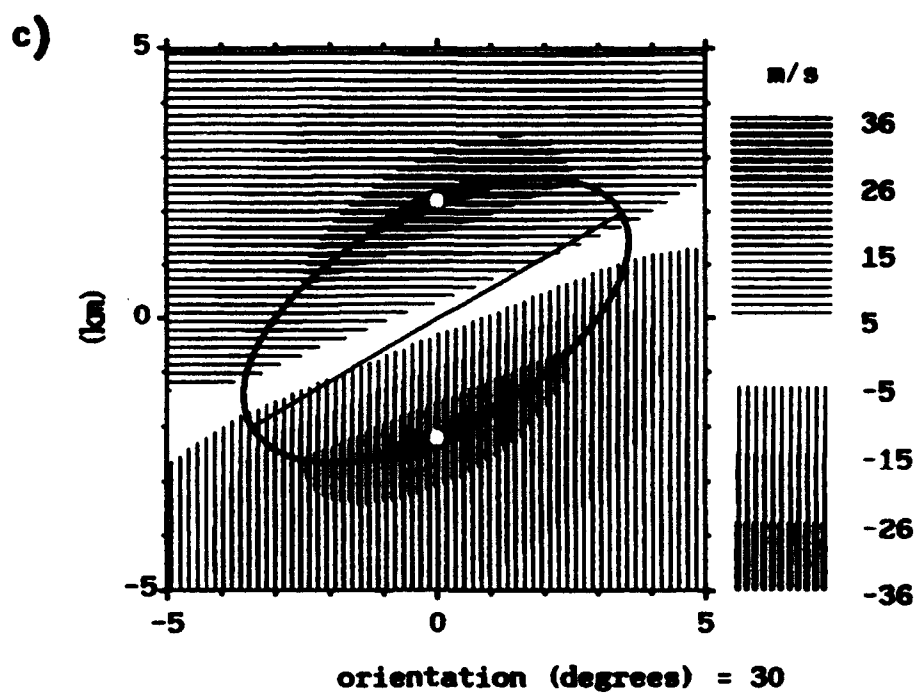


Figure 16. (Continued)

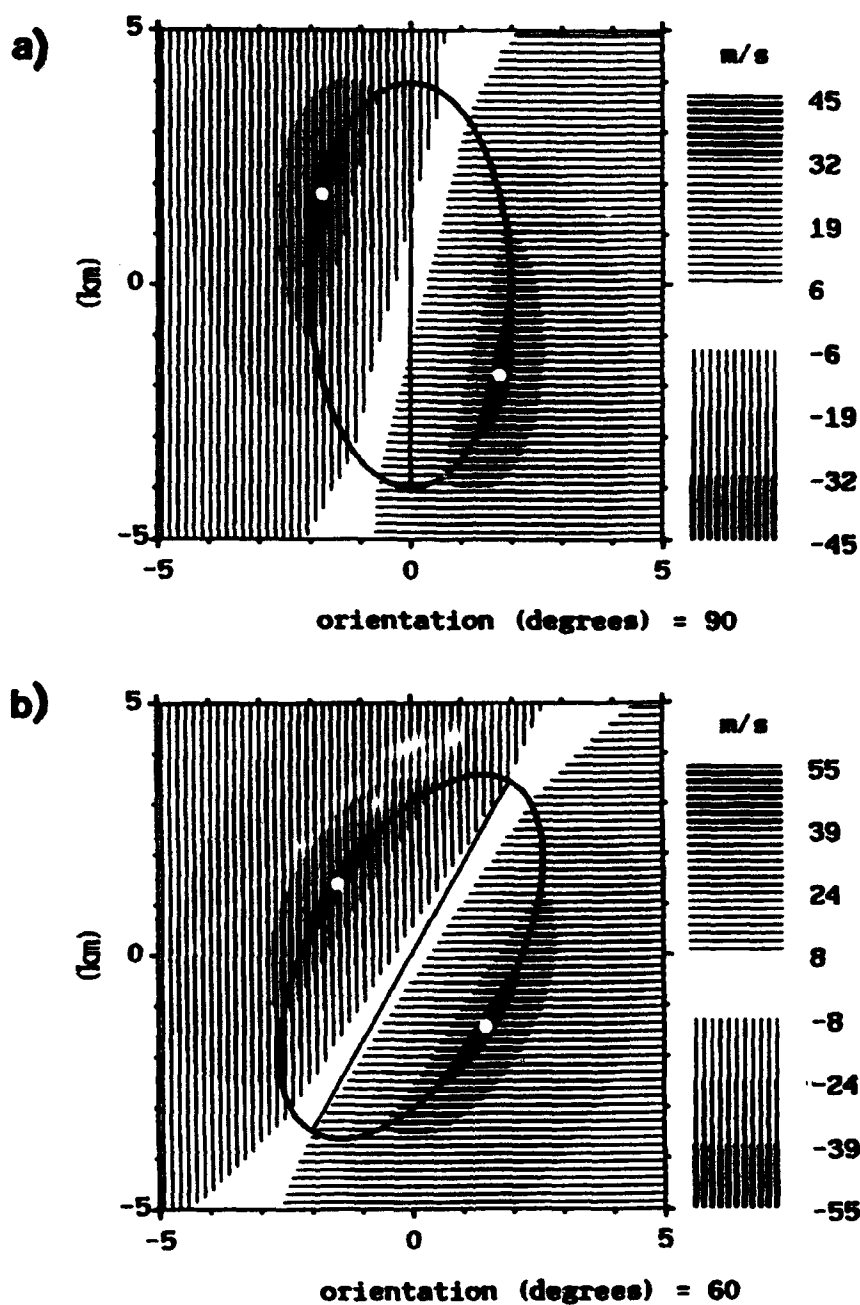


Figure 17. Examples of the Elliptical Mesocyclone Model Velocity Field for Equal Magnitudes of Convergence and Vorticity Inside the Core. The viewpoint is that of a single-Doppler radar, located towards the bottom of the page. Contour levels are as indicated in Figure 1. White circles indicate the precise location of velocity maxima. Example shown is for an ellipse of stretch factor (S) = 2. Ellipse size, shape, and orientation relative to the radar are indicated by the thick solid line. The straight line bisecting the ellipse is along the major axis. The examples, a,b,c, and d are for the same feature observed at a feature orientation angle (θ_f) of 90, 60, 30, and 0°, respectively.

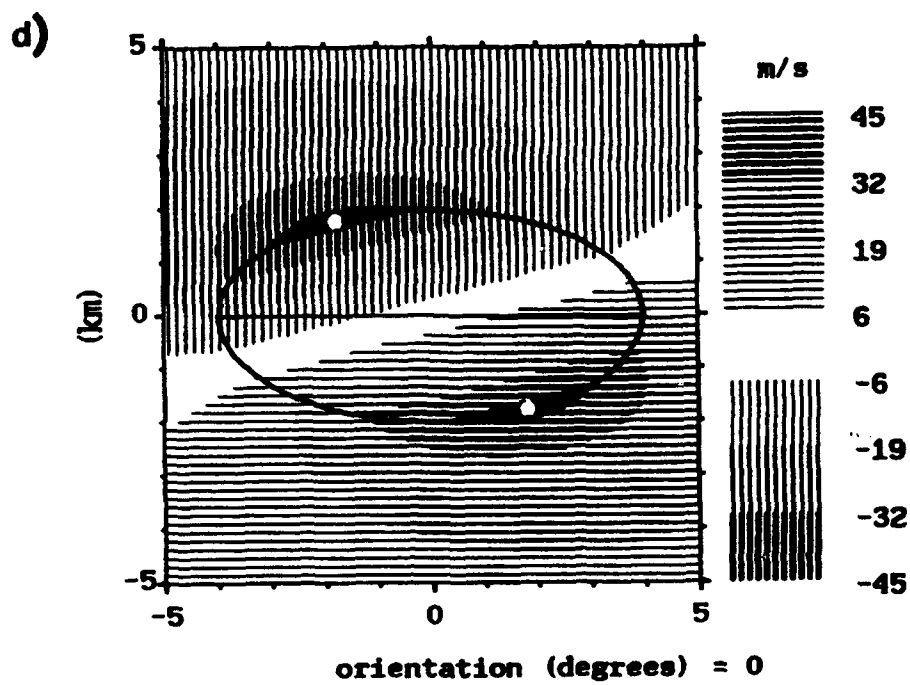
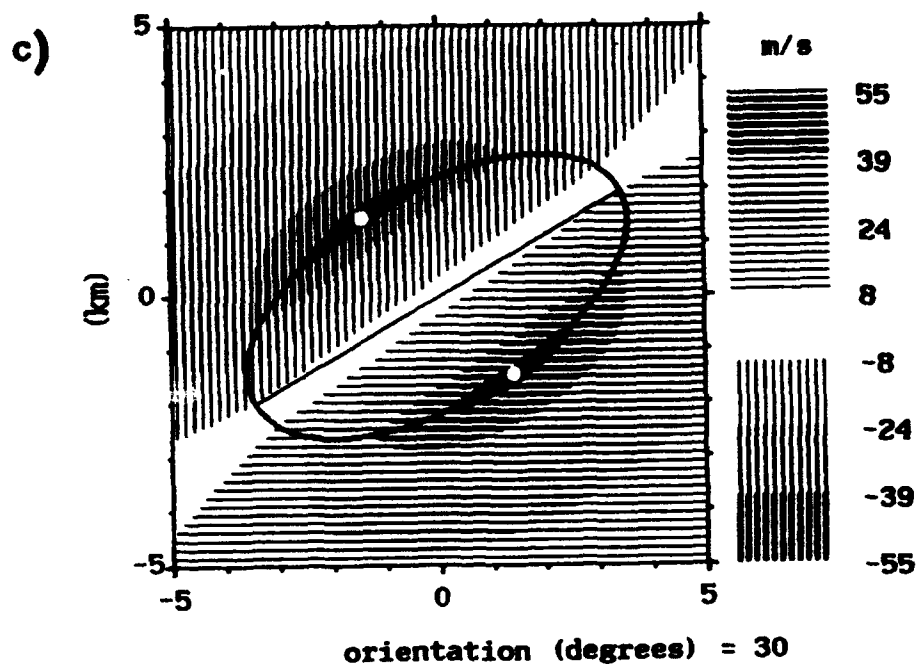


Figure 17. (Continued)

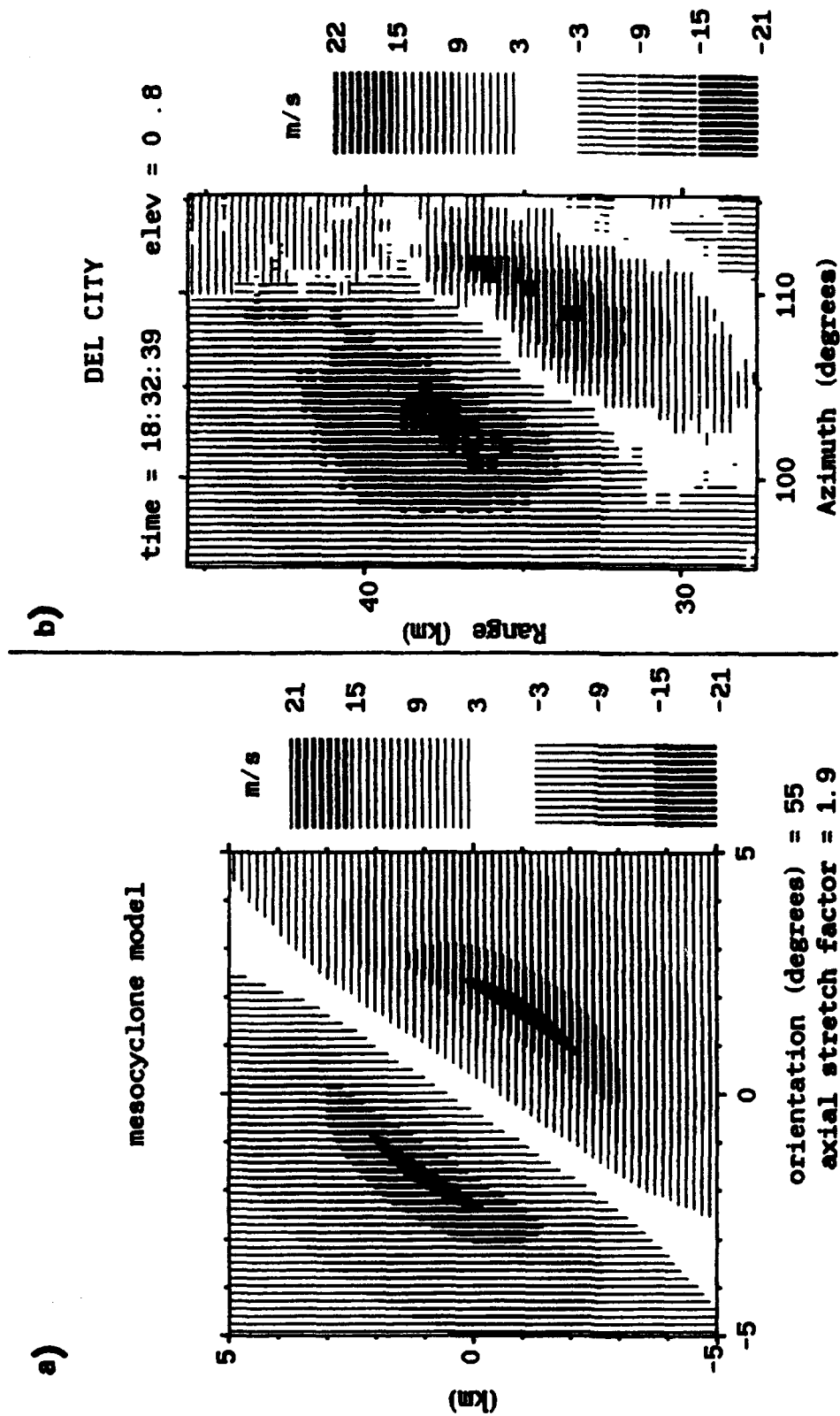


Figure 18. Comparison of the Elliptical Mesocyclone Model a) to an example from the Del City storm (b). Each show a flow field comprised of a combination of convergence and rotation. The Del City example is estimated to have a stretch factor (S) of 1.9, is oriented at $\theta_f = 55^\circ$ and convergence within the core is equal to 0.6 of the vorticity. The model example represents these same characteristics. Presented scales of size are somewhat different. Contour levels are as indicated in Figure 1.

flow from one side of the mesocyclone to the other, which is not included in the model. Velocities on the right side (figure relative) of the Del City mesocyclone change at a rate greater than potential flow. The opposite is true of the left side. Clearly, in the examples seen up to now, only the core region fits our simple model.

4.3 Non-Uniform Convergence

In previous sections, the investigation has addressed conditions where uniform vorticity and divergence fields exist in the mesocyclone core region. In this section, the condition of non-uniform fields is addressed. Non-uniform convergence is likely to exist, for example, at low levels of a storm where the inflow is unidirectional. Natural variations in inflow patterns are likely innumerable. It is helpful to examine cases where the vorticity and divergence fields are known.

In the Brandes (1984) multiple-Doppler study,⁷ aspects of the flow of the Del City storm are revealed. Figure 19a shows his analysis of the convergence term contributing to vorticity tendency at 1.3 km AGL and 1826 CST (here, north is towards the top of the figure). Also shown is the vertical vorticity at the same height (Figure 19b). The dashed line in each figure indicates the mesocyclone outline as defined by vorticity $\geq 0.01/s$. The thick solid line is the mesocyclone outline determined through single-Doppler analysis. Both of these indicate an elliptical flow pattern. In this example of the Del City mesocyclone, vorticity was non-uniform in the "core" region, peaking inside the core in a region southeast of the geometric center.

A perspective of the inflow is obtained from the convergence term (Figure 19a), given by $(\partial u_x/\partial x + \partial u_y/\partial y)$ ($\partial u_y/\partial x - \partial u_x/\partial y$). The convergence term of the vorticity tendency equation is not necessarily representative of the wind field convergence. However, if vorticity is uniform the convergence term will indicate the distribution of divergence, although not the magnitude. Figure 19b shows that vorticity is not uniform in the core. However, this may be the result of a non-uniform inflow, since the vorticity peak is off-center from the mesocyclone ellipse. This contention will be supported if the shape and magnitude of the convergence term seen in Figure 19 a and b can be simulated by including rotation derived from the elliptical model that is centered at the ellipse geometric center and contains a constant horizontal mass flux.

The convergence field was simulated by trial and error, with guidance from the horizontal wind vectors (Figure 19c), which indicate convergence on the mesocyclone's east side. The most satisfactory reproduction is achieved when the maximum inflow is set at $\xi = 50^\circ$ and the minimum set at $\xi = 160^\circ$, with the mesocyclone minor axis ($\xi = 0^\circ$) oriented towards the NE. Furthermore, at $\xi = 160^\circ$ the wind field is slightly divergent such that the peak velocity due to divergence is 10 percent of the peak inflow value at $\xi = 50^\circ$. Therefore, the incoming velocity normal to the ellipse surface is approximated by the relationship:

$$V_d \{160^\circ < \xi < 50^\circ\} = a V_a \cos (|\xi - 50^\circ|/1.15) / R\{\xi\}. \quad (24)$$

For other angles,

$$V_d \{0^\circ \leq \xi \leq 50^\circ\} = a V_a \cos (\xi/2.61) / R\{\xi\}, \quad (25)$$

$$V_d \{160^\circ \leq \xi \leq 50^\circ\} = a V_a \cos ((\xi + 50^\circ)/2.61) / R\{\xi\}. \quad (26)$$

This relationship is applied from the mesocyclone geometric center, and velocity magnitudes vary linearly along any particular radial ξ .

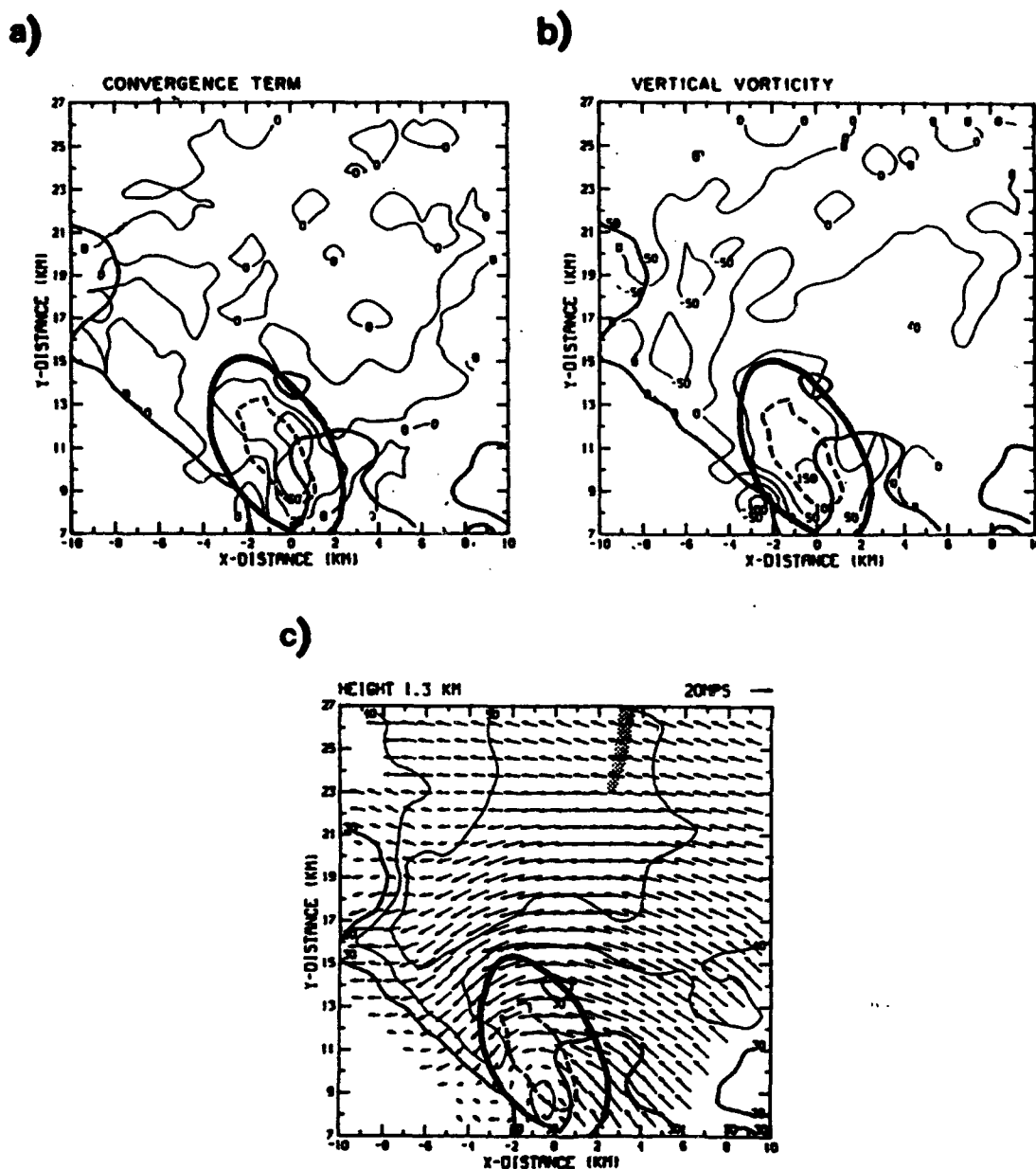


Figure 19. Fields of the Convergence Term of the Vorticity Tendency Equation (a), Vertical Vorticity (b), and Low Level Winds (c) Determined From Multiple-doppler Analysis of the Del City Storm at 1826 CST and 1.3 km AGL (adapted from Brandes,⁷). The convergence term has units of $10^{-6}/s^2$. Vorticity units are $10^{-4}/s$. In (c), horizontal wind vectors are shown with radar reflectivity superimposed, and the stippled area towards the top of the figure indicates the region of subsequent tornado damage that began 14 minutes after this time. The medium-thickness solid line reproduced in each figure is the 30 dBz reflectivity contour. The dashed line in each is the objectively determined mesocyclone, corresponding to the $0.01/s$ vorticity contour. The thick solid line surrounding this is the mesocyclone outline determined from subjective analysis of the single-Doppler velocity field.

The simulated convergence-term field for the mesocyclone area of Figure 19a is shown in Figure 20. This represents an ellipse of stretch factor (S) = 2.0 with the peak inflow and rotational velocities adjusted to approximate the convergence term field of the multiple-Doppler analysis. As in Figure 19, the orientation of the field is presented to correspond to its geographic orientation and not to the radar. Although the simulated field is not as detailed as the true field, it is representative in magnitude and general appearance.

The corresponding divergence field is shown in Figure 21. Convergence in the core region is greatest on the mesocyclone's eastern side, and there is slight divergence in the southwestern quadrant. One aspect that is not well represented is the region of potential flow. This is especially apparent in the northeast quadrant where the flow is divergent. No attempt is made here to improve the representation of the potential flow since the immediate results concern only the flow inside the core.

One effect of a non-uniform convergence field in the core is an induced vorticity field, shown in Figure 22. The resultant vorticity field from the combined fields of induced vorticity and vorticity of pure rotation is shown in Figure 23. In this simulation, vorticity is largest in the southeast quadrant of the mesocyclone core, in general agreement with the multiple-Doppler derivation (Figure 19b). The simulation underestimates the peak in vorticity by 15 percent, however.

Also represented in the simulation is the region of anticyclonic vorticity in the potential flow region to the southwest of the mesocyclone core. Little significance is attached to this since the potential flow region is not modeled well. It can be argued that the vorticity distribution in the potential flow region may be due, in part, to the inflow field, since that is what is observed in the core. However, at higher elevations of the Del City storm at this same time, there is evidence in the single-Doppler observations that a rear-flank downdraft is forming, characterized by an anticyclonic velocity couplet (not shown). A developing rear-flank downdraft may also have contributed to the high value of anticyclonic vorticity seen in the multiple Doppler analysis. There is no evidence in the multiple Doppler analysis to support the region of anticyclonic vorticity indicated by the model to the northeast of the mesocyclone core.

The single-Doppler B-scan view of the multiple-Doppler analysis is shown in Figure 24 along with the model simulation. This is a radar perspective from the west of the mesocyclone. The thick line in the model indicates primary inflection points along the velocity contours and outlines the mesocyclone core, with a stretch factor of approximately 2.0. One distinctive character of this example is the shifting of the velocity peaks so that they lie at one end of the core region, a result of the increased convergence and vorticity there. The model simulation is similar. All the major components of the flow are represented, from the shifting of the velocity peak locations to the elongation of the contours on the "right" side of the mesocyclone. The one characteristic of the simulation that is not well represented is the bending, or "S" shape, of the zero-line seen in the real-life example. The generally straight zero-line of the simulation is a result of applying a linear variation of velocity in the core region along a given radial ξ . It is possible to maintain a constant horizontal mass flux for rotation with velocity varying other than linearly. The result would be that vorticity in the core would not be uniform but a ring of maximum vorticity would exist somewhere within the core or could peak near the mesocyclone center. This scenario would account for the S pattern seen in the real data and would explain why vorticity was underestimated in the simulation. It also explains why the mesocyclone size by vorticity magnitude from Brandes⁷ is significantly different from the single-Doppler estimation of the core (Figure 19b).

In summary, a directional and non-uniform inflow field was superimposed upon an otherwise uniform rotation field that is described by a simple elliptical model. The non-uniform inflow produced non-uniform divergence in the mesocyclone core region, and, more to the point, contributed to the vorticity field, making it non-uniform as well.

5. DISCUSSION AND CONCLUSIONS

To the author's knowledge, all single-Doppler work of mesocyclones to date has been based on the assumption that the mesocyclone can be approximated by a circular flow. This work details an improvement on that model that accounts

convergence term of vorticity tendency

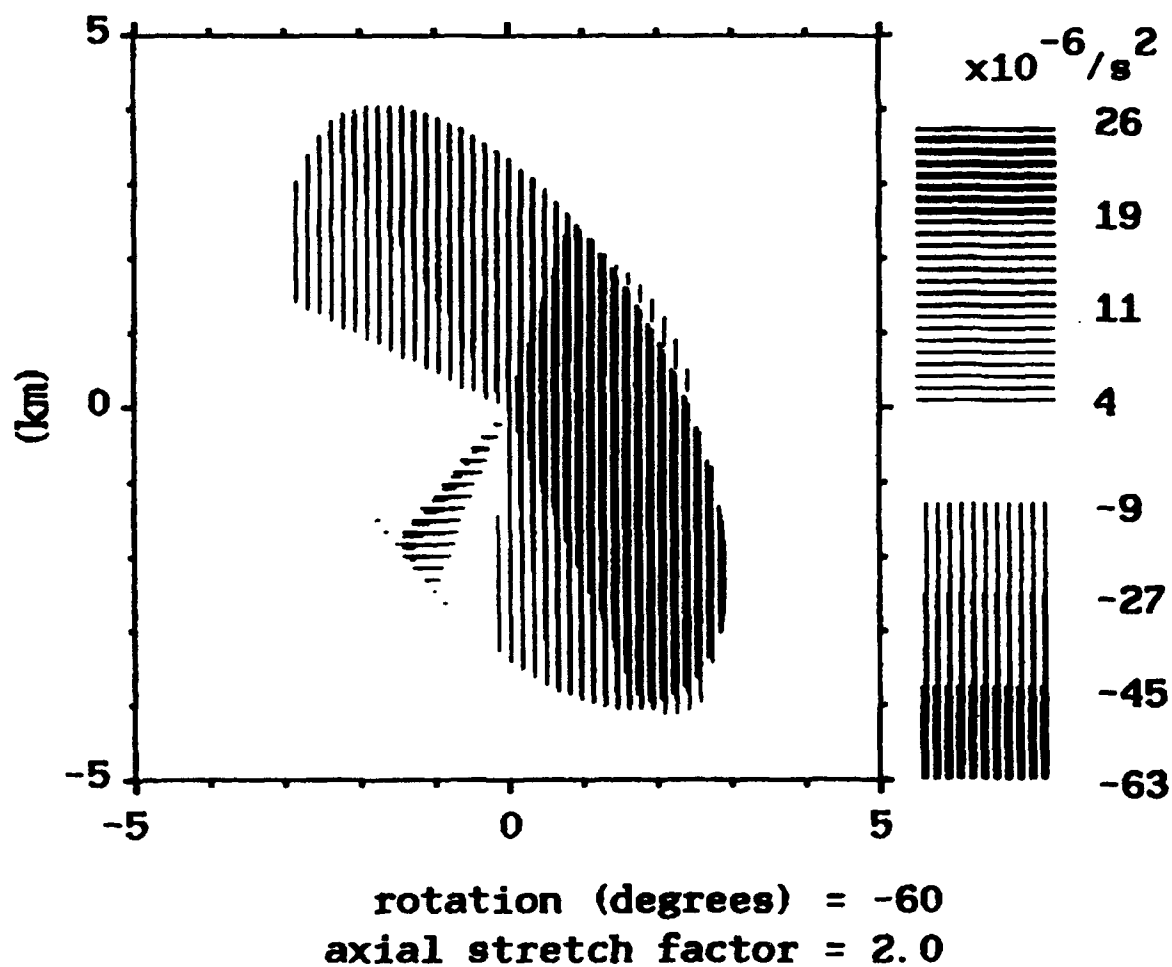


Figure 20. A Simulation of the Convergence Term of the Vorticity Tendency Equation for the 1826 Del City Example of Figure 19a. The mesocyclone orientation in this case (-60°) corresponds to its geographic orientation, as in Figure 19, and not to the orientation with regards to a radar.

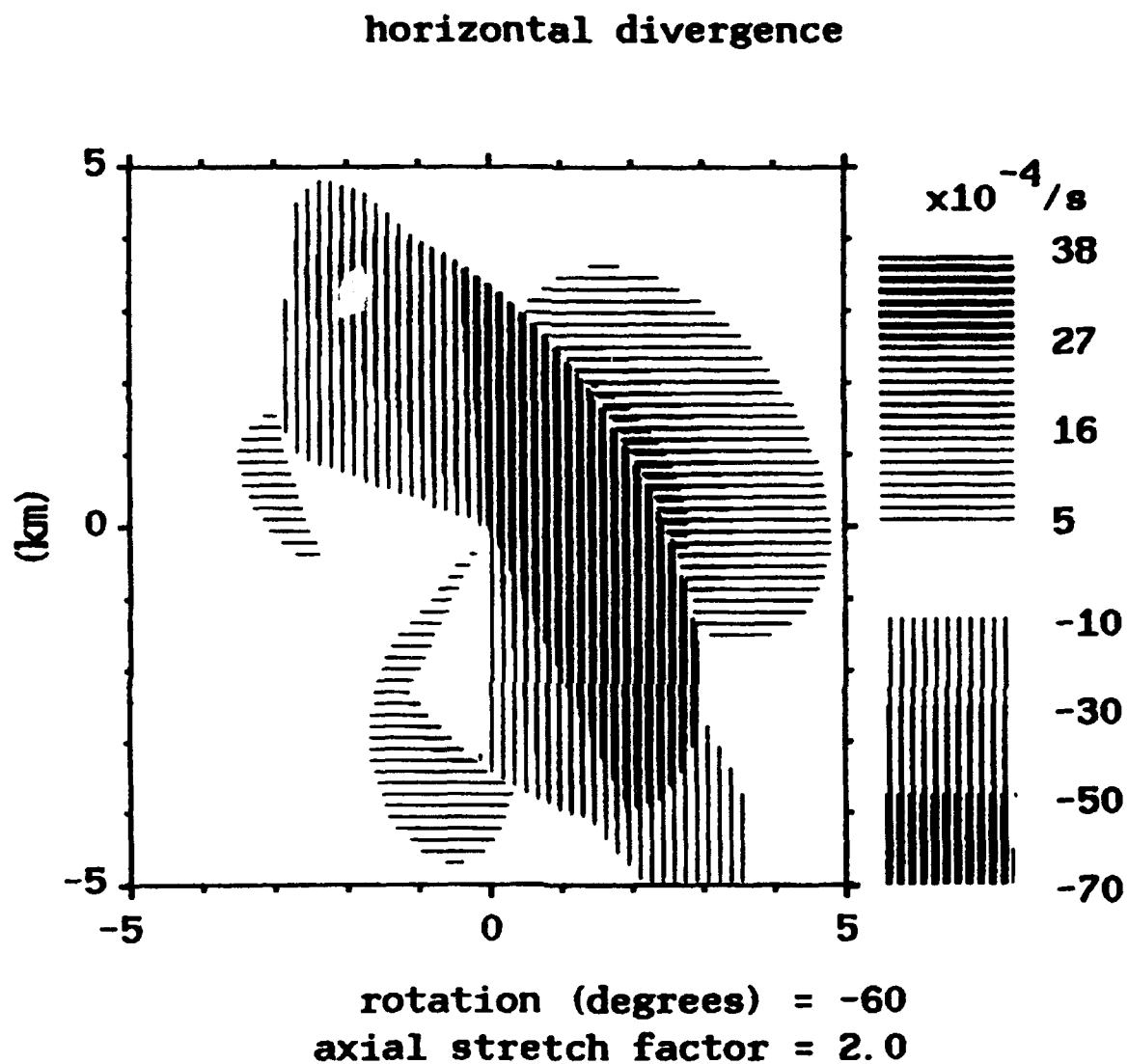


Figure 21. The Divergence Field Contributing to the Convergence Term of Vorticity Tendency Shown in Figure 20.

inflow-induced vertical vorticity

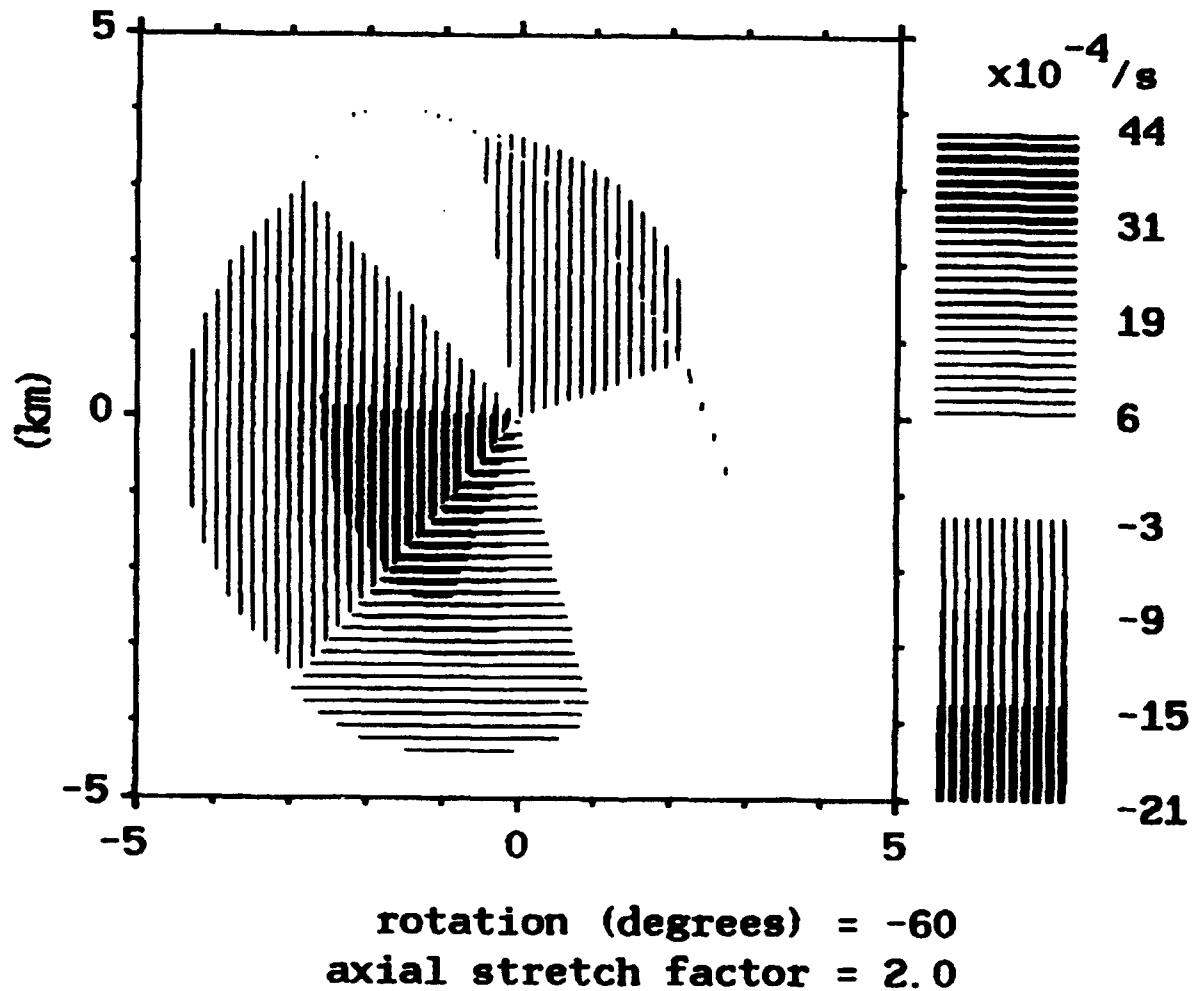


Figure 22. The Induced Vorticity Field Associated With the Non-uniform Inflow of Figure 21.

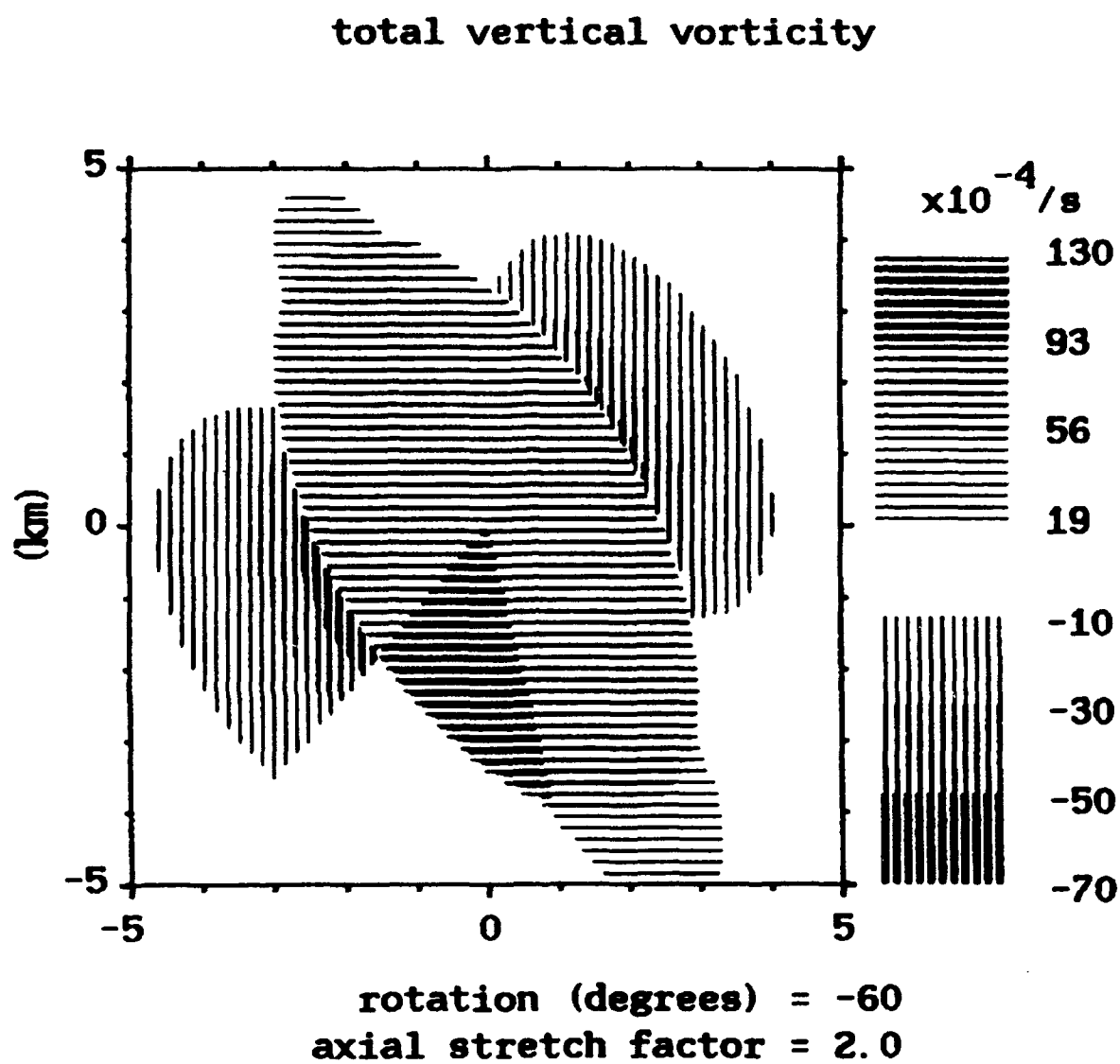


Figure 23. The Total Model Vorticity Field From the Combination of a Uniform Vorticity Field for Rotation With the Vorticity Induced by the Non-uniform Inflow.

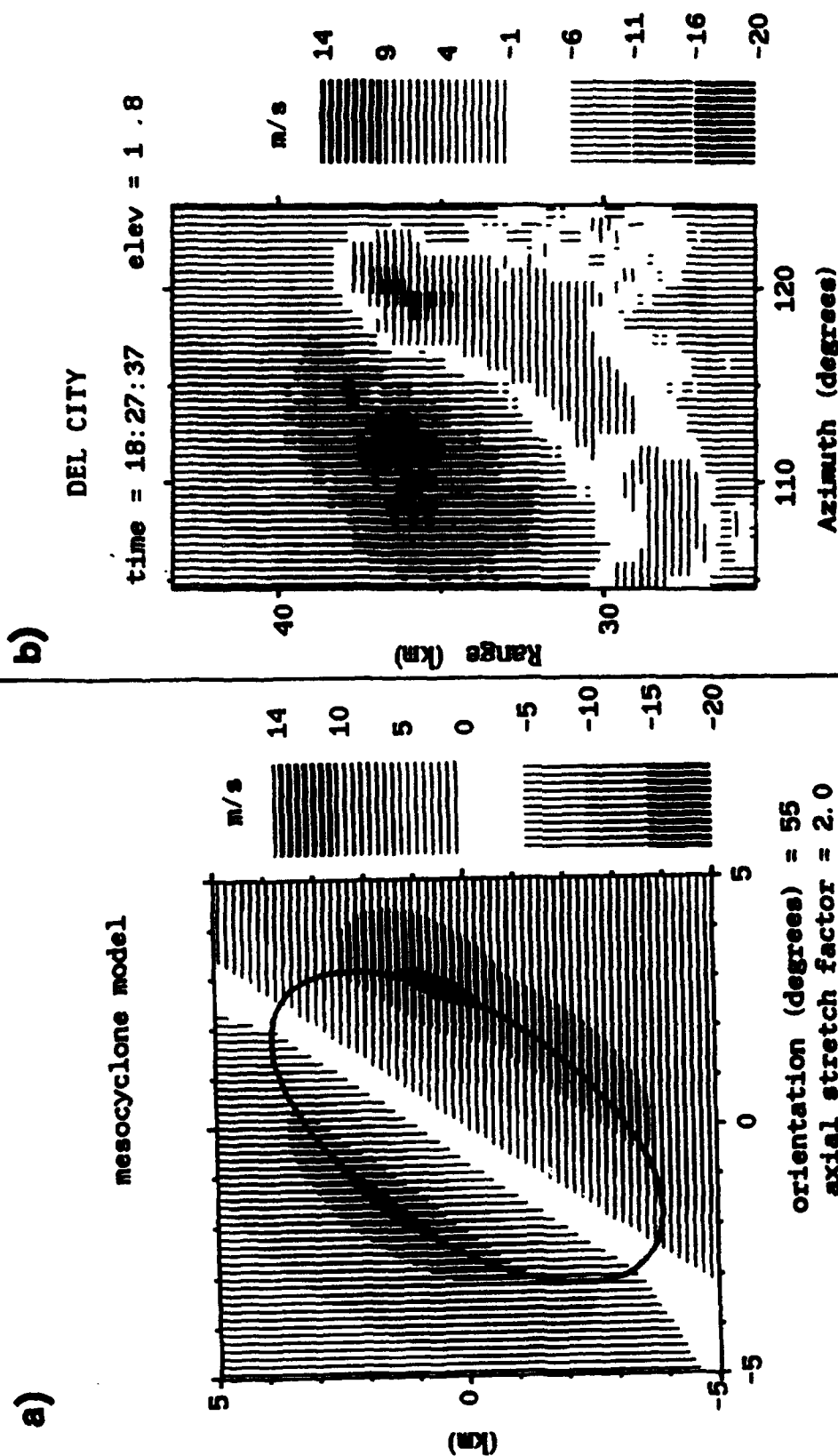


Figure 24. An Example of How the Model Can be Used to Explain Complicated Patterns of Vorticity and Divergence in the Mesocyclone Core. b) The single-Doppler view of the Del City mesocyclone associated with the fields of Figure 19. It is oriented at $\theta_r = 55^\circ$ with regards to the radar, and has a stretch factor of 2.0. a) A simulation of the Del City case from combining the estimated vorticity and divergence fields of Figures 21 and 23. The thick solid line in the shape of an ellipse indicates the mesocyclone outline. The thinner line bisecting the ellipse is along the ellipse major axis. Countouring in a) and b) is consistent with Figure 1. In this model example, a general field of rotation is assumed where there is uniform vorticity in the core and constant horizontal mass flux. Overlaid on this is a field of non-uniform convergence.

for the observed elongation of many mesocyclone flows. This new model does not negate the concept of a circular mesocyclone, but is rather an extension of the original Rankine-Combined vortex flow.

Some examples of elongated mesocyclone flows observed with single-Doppler radar are presented. These are closely simulated by a two-dimensional elliptical model that has a simple kinematics structure. The general model is one in which vorticity and divergence are both uniform within the core, a quality associated with the conventional "circular" mesocyclone model. One deviation from the circular mesocyclone model is a couplet of anticyclonic vorticity in the potential flow region of a cyclonically rotating elliptical mesocyclone. The intensity of the anticyclonic couplet increases with increasing elongation of the ellipse.

An important caveat of elliptical flows is that the detected rotational shear varies as a function of the ellipse orientation to the radar. The ratio of the maximum to minimum rotational shear within the ellipse varies according to twice the ellipse stretch factor. For the Del City example discussed herein, where the major axis is 1.8 times the minor axis length, the detected radial shear would vary by 360 percent around the mesocyclone perimeter if the flow were perfectly modeled by an ellipse. The problem is that the established criteria for mesocyclone detection assume that the mesocyclone flow is approximately circular.¹¹ Therefore, early detection of mesocyclonic shear, or detection of weak mesocyclones at all, is very much dependent on viewing angle. Either the criteria for mesocyclone detection need to be modified, or methods to infer peak shear in elliptical flows need to be developed.

Excess rotational kinetic energy suffers from the same viewing angle problem as shear. Unless the eccentricity is known, the ERKE may be underestimated or overestimated considerably: by a factor of 2 or more for even moderate eccentricity with a stretch factor of 1.5. For a mid-level, elliptical mesocyclone, where the flow field consists solely of rotation, the orientation angle where circular flow can be assumed with minimal error in estimating ERKE is about 45 degrees. For the Del City, Oklahoma storm examined, with an inflow from the SE and the mesocyclone major axis oriented NNW to SSE, the best viewing angle to determine ERKE is with the storm generally east or west of the radar. Clockwise (counterclockwise) of these directions ERKE would be overestimated (underestimated) if the flow were approximated by a circle. It would be worthwhile to determine the general orientation of elliptical flows.

Rotational kinetic energy can be determined accurately regardless of ellipse viewing angle for an elliptical flow by assuming the detected peak velocities belong to a circular flow. Unfortunately, RKE has not been found useful for mesocyclone classification or for determining severe storm potential.

The model describes a two-dimensional flow in what is, in reality, a three-dimensional flow field. It is easier to apply constraints to the generally horizontal rotation field than to the divergence field, because with horizontal divergence, mass continuity requires a direct translation to vertical motion. Constant horizontal mass flux for rotation appears to be a valid and useful assumption for the interpretation of the mesocyclone. In examples presented herein, the application of various divergence fields to a uniform vorticity field closely reproduces the observed single-Doppler flow field. A good test of the concept of constant horizontal mass flux for rotation is provided by a multiple-Doppler analysis of the Del City, Oklahoma mesocyclone by Brandes.⁷ His analysis generated the actual vorticity and divergence fields, which can be used as inputs to the model. With a constant vorticity in the core due to rotation, the non-uniform divergence field from the multiple-Doppler analysis is applied. Interestingly, the inflow field accounts for the observed irregularities of the vorticity field. The resulting single-Doppler simulation closely resembles the observed real-life example. This increases confidence that the model is realistic.

The limited perspective offered by single-Doppler radar can make it difficult to interpret the mesocyclone flow. It is possible to retrieve more accurate flow estimates by applying more realistic models. With the ultimate goal of applying automatically such a model as presented here, much work needs to be done. Present mesocyclone detection algorithms for NEKRAD do not account for elliptical flow in their estimations. The results presented herein show that this shortcoming can have dire consequences in terms of mesocyclone detection and severe weather evaluation.

References

1. Lhermitte, R. M (1964) Doppler radars as severe storm sensors. *Bull. Amer. Meteor. Soc.*, 45:587-596.
2. Donaldson, R. J., Jr., (1970) Vortex signature recognition by a Doppler radar. *J. Appl. Meteorol.*, 9:661-670.
3. Wieler, J. G. (1986) Real-time automated detection of mesocyclones and tornado vortex signatures. *J. Atmos. Oceanic. Technol.*, 3:98-113.
4. Zrnic', D. S., Burgess, D. W., and Hennington, L. D. (1985) Automatic detection of mesocyclonic shear with Doppler radar. *J. Atmos. and Oceanic Technol.*, 2:425-438
5. Witt, A. and Nelson, S. P. (1991) The use of single-Doppler radar for estimating maximum hailstone size. *J. Appl. Meteorol.*, 4:425-431.
6. Desrochers, P. R. and Donaldson, R. J., Jr. (1992) Automatic tornado prediction with an improved mesocyclone-detection algorithm. *Wea. Forecasting*, 7:373-388.
7. Brandes, E. A. (1984) Vertical vorticity generation and mesocyclone sustenance in tornadic thunderstorms: the observational evidence. *Mon. Wea. Rev.*, 112:2253-2269.
8. Brown, R. A., and Wood, V. T. (1991) On the interpretation of single-Doppler velocity patterns within severe thunderstorms. *Wea. Forecasting*, 6:32-48.
9. Wood, V. T. (1991) *Mesocyclone data compared with a mesocyclone model*. NSSL in-house report.
10. Fujita, T. T. (1981) Tornadoes and downbursts in the context of generalized planetary scales. *J. Atmos. Sci.*, 38:1511-1534.
11. JDOP Staff (1979) *Final report on the Joint Doppler Operational Project (JDOP) 1976 - 1978*. NOAA Tech. Memo., ERL NSSL - 86, 84 pp.
12. Donaldson, R. J., Jr. and Desrochers, P. R. (1990) Improvement of tornado warnings by Doppler radar measurement of mesocyclone rotational kinetic energy. *Wea. Forecasting*, 5:247-258.
13. Desrochers, P. R. (1990) Some aspects of the mesocyclone related to hail formation. Preprints, *16th Conf. on Severe Local Storms*, AMS, Boston, MA, 246-251..

14. Donaldson, R. J., Jr. and Desrochers, P. R. (1985) Doppler radar estimates of the rotational kinetic energy of mesocyclones. Preprints, *14th Conf. on Severe Local Storms*, AMS, Boston, MA, 52-55.
15. Burgess, D. W., Wood, V. T., and Brown, R. A. (1982) Mesocyclone evolution statistics. Preprints, *12th Conf. on Severe Local Storms*, AMS, Boston, MA, 422-424